sustainability

MDPI

Review

Plasma Technology and Its Relevance in Waste Air and Waste Gas Treatment

Christine Dobslaw * and Bernd Glocker

PlasmaAir AG, Weil der Stadt, 71263 Hausen, Germany; glocker@plasmaair.de

* Correspondence: dobslaw@plasmaair.de; Tel.: +49-7033-30988-48; Fax: +49-7033-30988-50

Received: 15 September 2020; Accepted: 20 October 2020; Published: 29 October 2020



Abstract: Plasma technology is already used in various applications such as surface treatment, surface coating, reforming of carbon dioxide and methane, removal of volatile organic compounds, odor abatement and disinfection, but treatment processes described in this context do not go beyond laboratory and pilot plant scale. Exemplary applications of both non-thermal plasma and thermal plasma should underline the feasibility of scale-up to industrial application. A non-thermal plasma in modular form was built, which is designed for up to 1000 $m^3 \cdot h^{-1}$ and was successfully practically tested in combination of non-thermal plasma (NTP), mineral adsorber and bio-scrubber for abatement of volatile organic components (VOCs), odorous substances and germs. Thermal plasmas are usually arc-heated plasmas, which are operated with different plasma gases such as nitrogen, oxygen, argon or air. In recent years steam plasmas were gradually established, adding liquid water as plasma gas. In the present system the plasma was directly operated with steam generated externally. Further progress of development of this system was described and critically evaluated towards performance data of an already commercially used water film-based system. Degradation rates of CF_4 contaminated air of up to 100% where achieved in industrial scale.

Keywords: non-thermal plasma; thermal plasma; dielectric barrier discharge; DBD; water steam plasma; waste gas treatment; plasma technology; waste air treatment

1. Introduction

Plasma is the gaseous fourth state of matter, which is created by the supply of energy in addition to the states of solids, liquids and gases, in which charges are separated from each other in a stable form. This meta-stable state can be generated by thermal energy but is mainly generated by supplying electrical energy in technical plasmas. Natural occurrences of plasmas include lightning, aurora borealis, or the corona of the sun [1].

The first experiments with technical plasmas were conducted as early as 1705 by Francis Hauksbee, who generated arcs of light in evacuated glass spheres [2]. These are still known today as decorative plasma spheres or lamps.

A technical application of plasmas was firstly reported in 1857 by Werner von Siemens, who developed an ozonizer to treat drinking water with ozone [3]. The plasma as such was named in 1928 by Irving Langmuir [4].

Today, plasmas are used in many different areas; as examples in households in the form of gas discharge lamps (energy-saving lamps, neon tubes) and plasma televisions, in industrial for surface treatment (plasma polymerization), analysis technology (plasma ashing), medicine (disinfection, wound treatment) and food industry (disinfection) [5–7]. The possible applications of plasmas are manifold and have been used in environmental technology since the 1980s. Non-thermal plasmas, for example, were already used in 1984–1986 for the treatment of military waste. [8,9]. Since then research in plasma sciences focused on geometries of plasmas, test plants and electrodes; search for

capable material for construction of plants, electrodes, and barriers; power supply; plasma gases and the selection and optimization of catalytic materials as in-plasma catalysis (IPC) or post-plasma catalysis (PPC) [10–12]. However, based on recent publications, research dominantly focuses on bench-scale plasmas of very small system volumes (a few mL) and exhaust air flows (a few mL·min^{-1} to L·min^{-1}) [13,14]. The scale-up factors and operating costs derived from this scale are mostly doubtful or far beyond economically interesting applications. Since plasmas are mostly used for the treatment of hardly degradable pollutants or mixtures, they are in direct competition with incineration processes. Here, the operating costs are essentially defined by the consumption of fossil fuels, which in turn can be directly derived from the temperature difference between clean and crude gas. Modern combustion processes work with a temperature difference of 35 K (in case of crude gas levels above 90 °C) or 50 K (crude gas of ambient temperature). Depending on the quality of the natural gas and neglecting both latent heat losses and energy requirements for compressors and compressed air, this change in temperature corresponds to a specific input energy (SIE) value of 16.0–21.0 kWh·1000 m^{-3}, which must be used at least as indicator of economic efficiency of non-thermal plasma (NTP) processes.

In this article, the experiences with non-thermal and thermal plasmas on a pilot and industrial scale and their importance for waste air and waste gas purification will be discussed in detail on the basis of own research results of the last years.

2. Non-Thermal Plasma

2.1. Designs and Operational Parameters

As shown above, plasmas can either be generated by supplying thermal energy or electrical energy in the form of kinetic energy. Technical designs of non-thermal plasma include dielectric barrier discharge (DBD), gliding arc, microwave discharge, glow discharge, corona discharge and radio frequency discharge, which were previously described in detail [13,15,16]. The most commonly used method of NTP in pilot- and industrial scale is the dielectric barrier discharge technology. Here, a sufficiently high electrical voltage is applied between two electrodes to ionize the intermediate gas. To prevent a breakdown by arc discharge, the two electrodes are galvanically separated by a dielectric barrier. After the plasma is ignited, the charges flow in the direction of the electrodes or dielectric barrier, depending on their polarity. Since the dielectric barrier is insulating, the charges cannot flow off and accumulate on the surface. An opposing electric field is thus formed, which causes ceasing of the discharge. By change of polarity, the plasma can be re-ignited. Overall, only surface charges are exchanged in DBD between the electrodes and the dielectric barrier. This corresponds to a displacement current through which electrical power is transferred into the plasma. Changes in polarity take place at frequencies of a few hundred Hz to MHz at up to 30 kV of applied voltage. Only the light electrons in the discharge zone can follow this high frequency, while the heavier cations are hardly accelerated or the momentum changes due to their mass inertia. The electron temperature is thus significantly higher than the heavy particle temperature, which ensures reactivity in the plasma due to the high-energy electrons, and the gas temperature does not increase significantly and remains in the range of the original waste gas temperature. Non-thermal plasmas are therefore not in thermodynamic equilibrium. The effectiveness of the DBE lies in the selective energy coupling into the released electrons, which are accelerated by the electric field to energies between 1 and 10 eV and are subject to a number of reaction mechanisms in the plasma, which were previously described in detail [17,18]. As a consequence of these reaction mechanisms, radicals, negative ions, positive ions, or metastable molecules are formed in humid air as carrier gas out of oxygen, nitrogen and water molecules in different excitation states with different reactivity and lifetime.

The detailed composition and design of the electrodes and barriers in DBD both depends on the type of application and the required process stability. This stability, as well as the energy efficiency of the NTP process, is negatively influenced by high humidity, dust and waste gas components that tend to polymerize or form a coating during plasma exposure [19]. The effect of the electrode structure, the

power supply, the packing materials of connected catalysts, and the effect of the gas properties on the discharge process itself were examined in detail by Li et al. [12].

Other forms of non-thermal plasma generation include corona plasmas, arc plasmas, electron beam discharges and plasma torches. In all of these alternatives the intermediate gas acts as an insulator. Since the insulating effect is low, transport channels of the ionized particles are formed (so-called streamers) so that the total discharge consists of a (multitude of) arc discharges. Negatively, occurring streamers cause high demands in electrical power up to a decade higher than for DBD and a heterogeneous plasma discharge. The latter aspect strongly affects the contact of waste gas compounds and reactive compounds in the plasma, and therefore, the efficiency of these alternative processes is generally lower than the efficiency of the DBE [16].

2.2. Aspects of Energy and Removal Efficiency

Both energy efficiency and removal efficiency of contaminants by the non-thermal plasma may be increased by combining the NTP with a catalytically active adsorber either used internally (so-called "in-plasma catalysis", IPC) or downstream (so-called "post-plasma catalysis"). By adsorption of the waste gas contaminants, exposure time of the pollutants towards reactive compounds is increased, and a significant acceleration of the reaction kinetics by physico-chemical interactions with the (photo-) catalytic surface may be observed. Due to the higher cleaning efficiency, IPC is preferably used compared to PPC, i.e., higher removal efficiencies may be achieved at fixed SIE values or the SIE value required for a cleaning task can be further reduced.

The efficiency of the radical production and the downstream conversion of the air pollutants mainly depend on process and operation factors as follows [10,11,17,18,20–29]: time gradient in current ($\Delta U/\Delta t$); frequency and amplitude of alternating current; SIE value; specific surface of the electrodes; curvature of the electrode surface; porosity of DBD materials; specifics of barrier materials; application and location of catalysts (IPC vs PPC vs no catalyst); applied catalytical materials; specific surface and particle size distribution of the catalyst; contact time within the plasma discharge; NTP operation in inflow or as bypass; reactor geometry; flow distribution and flow turbulence within the reactor; total pressure; temperature; polarity of the gas; chemical structure of the pollutants as well as concentrations of oxygen, ozone, water vapor, aerosols, CO_2 and air pollutants.

Energy efficiency was further increased by recent developments focusing on the use of alternating plasma [30] or via combinations with biological treatment steps [31]. In the latter case, the upstream NTP stage partially oxidizes the waste gas pollutants, making them more water-soluble and thus bioavailable (see Table 1). Since these secondary intermediates can be easily treated in the subsequent biological process, and this technique nearly operates neutral in CO_2 emissions and at significantly lower operating costs, these process combinations are of high ecological and economic interest. A review of the recent literature on this issue was recently published [32].

Table 1. Intermediates in non-thermal plasma (NTP) treatment of volatile organic components (VOCs).

Contaminant	Secondary Products	Reference
Methane	CO, CO_2, ethene, ethine, linear aliphatics up to C_6, methanol, ethanol, various aldehydes and ketone, dimethyl ether, methyl formate	[33,34]
Propane	formaldehyde, methyl nitrate, CO	[35]
Butane	CO, CO_2, acetone, acetaldehyde	[36]
Hexane	3-hexanol, 2-hexanol, 3-hexanone, 2-hexanone, 1-hexanol, hexane aldehyde	[37]
Dodekane	NO, NO_2, N_2O, CO_2, methane, ethene, ethine, various oxygenates	[38]
Cyclohexane	Cyclohexanone, cyclohexene, cyclohexanol, hexan aldehyde, 2-cyclohexenone	[37]
Dichloromethane	CO_2, CH_3Cl, $COCl_2$, HCl, Cl_2, HCOCl, NO, NO_2, N_2O	[39]
Ethylene	Formaldehyde, acetylene, CO, CO_2	[40]
Propene	Formaldehyde, CO, CO_2	[35]
Dibromomethane	CO, HNO_3	[18]
Chloroform	NO, NO_2, Cl_2, HCl, TCE, HCl	[41]
Trichloroethylene	Phosgene, COCl, CO_2, dichloroacetyl chloride, trichloro acetaldehyde, Cl_2, HCl, N_2O.	[42–45]
Trichloroethylene	CO	[46]
Freon	CClFO, $CHClF_2$, C_2ClF_2N, $CHCl_2F$, CCl_2FN, $COCl_2$	[47]
Methanol	Methane, formaldehyde, formic acid	[48]
Isopropanol	Acetone, formaldehyde, formic acid, CO, CO_2	[35,49]
Formaldehyde	HCO, formic acid	[50]
Isopentane aldehyde	Acetone, CO, CO_2	[51]
Butanone	Methyl nitrate, 2,3-Butanedien, CO2	[52]
Ethyl acetate	Ethanol, methanol, methane, formic acid, formaldehyde, CO, CO_2, NO_2, N_2O	[53]
Isobutyl acetate	Isobutane aldehyde, acetate, CO_2	[54]
Ethanediol	Acetaldehyde, formaldehyde, CO, CO_2	[55]
Cyclohexene	Cyclopentanone, cyclopentane carbaldehyde, 7-oxabicyclo(4,1,0)-heptane, cyclohex-2-enol, cyclohex-2-enone, 2-methylcyclopentanone, ethylidenecyclobutane, 2-ethylbut-3-en aldehyde, hexane dialdehyde	[56]
Limonene	Acetate and 25 other compounds	[57]
β–Pinene	Nopinone, 2-hydroxynopinone, formic acid	[58]
Toluene	Benzylalcohol, benzaldehyde, methylnitrophenol, formic acid	[59]
Toluene	Benzaldehyde, 3-methyl-2,5-furandione, ethanediol, acetate, formic acid	[57]
Toluene	Benzylalcohol, benzaldehyde, benzylformic acid, benzylacetate, tetradekane, hexadekane, heptadekane	[60]
Styrene	Benzene, toluene, benzaldehyde, phenylacetaldehyde, phenol, formic acid, acetophenone, phenyl acetate, phenylmethanol, phenylacetylene	[61]
Styrene	Benzene, toluene, benzaldehyde	[62]
Styrene	Benzaldehyde, phenol, phenylacetaldehyde, hexan aldehyde, heptane aldehyde	This study
Dimethyl sulfide	Methanol, carbonyl sulfide	[63]

2.3. Fields of Application

Supported by intensive research in the field of new catalyst development, DBD processes for treatment of surfaces, food, wastewater, wastewater disinfection, and waste gas have been in the focus of research in recent years [7,15,64–67]. It is noticeable that especially the application in environmental technology, here especially in the treatment of wastewater, increased. The efficiency of NTP processes for wastewater treatment is mostly simulated by water samples containing dyes, because the analytical evaluation can be done simply by photometric detection. Occasionally, pesticides such as dimethoates [64], pharmaceuticals, phenol or caffeine have also been successfully tested. However, while plasma treatment seems to be a promising route for removal of organic pollutants from water, corresponding NTP degradation pathways are still not understood [64].

Application of DBEs in the field of fiber surface treatment and reforming of methane is also increasing [15]. Applications in waste gas treatment mainly focused on the disinfection of food, food storage rooms, surfaces and VOC abatement [68].

2.3.1. Methane Reforming

Methane reformation is a highly topical issue. Methane is one of the greenhouse gases and is considered as a source for the production of hydrogen. Methane turnover has to been seen in context with plasma-induced reactions of CO_2, where CO, H_2, methane and methanol and longer-chain products like ethane, ethene, ethine or propene [69,70] can be formed by dry reforming of methane, CO_2 hydrogenation, CO_2 reduction with water and CO_2 decomposition, and hence, plasma treatment is a promising technology for CO_2 capturing, too [15,67,71,72]. Therefore, many research groups deal with the plasma-assisted production of hydrogen from methane and synthesis gases, considering both non-thermal and thermal plasmas as conversion technology [15,73–76].

The use of non-thermal plasma is subject to a limitation: methane is inert and requires at least 1000 °C to cleave the C-H bond [70]. Hence, efficiency in transformation of educts (CO_2, CH_4) and formation of products (H_2, CO) during dry reforming of methane extremely depends on the SIE values, which are reported in the range of 3333–225,000 kWh·1000 m^{-3} [15,67,71]. As consequence, economic and ecological advantages cannot be derived directly due to high energy costs and secondary emissions of CO_2.

In order to use non-thermal plasma for methane reforming at all, catalysts are needed that reduce the starting temperature of methane to 50–300 °C [12]. Montoro-Damas et al. [77] were able to achieve a transformation efficiency of 47.5% in pure methane atmosphere still at high SIE values of 138.900 kWh·1000 m^{-3}, but considering lower methane concentrations of 2500 ppm, conversion of 32.5% of the methane were achieved at conditions of 50 °C, 0.14 s contact time and a SIE value of 165 kWh·1000 m^{-3}. Conversely, the inert character of methane can be used to purify methane in biogas or biomass gasification applications by NTP processes [78].

2.3.2. Odor Removal

One application predestined for NTP technology is odor abatement, since low SIE values are required due to the low concentration of odorous components, which means that the process can be used very successfully and cost-effectively. For example, Mizuno et al. (2007) [79] described a reduction in odor of at least 90% in the case of H_2S emissions from a rubber plant at a contact time of up to 3.3 s and an SIE value of 0.86 kWh·1000 m^{-3}. In the case of a spice factory, an odor reduction of 80–90% could already be realized at a SIE value of 0.1 kWh·1000 m^{-3} with an odor concentration in the inlet of 100,000 OU·m^{-3}. Müller and Zahn (2007) [80] described the treatment of an waste gas from a French fries factory by different DBD process variations. Three of four DBD modifications were able to achieve clean gas levels of less than 500 OU·m^{-3} at 13,000 OU·m^{-3} in the crude gas and thus comply with the specifications of the German Technical Instruction on Air Quality Control. The efficiencies were 97.2–98.7%. However, no data on energy consumption was provided.

A number of other publications describe emissions of odorous components such as ammonia and dimethylamine as representatives for nitrogenous compounds or hydrogen sulfide, carbon disulfide or dimethyl sulfide as sulfur-containing compounds, resulting in odorous concentrations between 1100 OU·m^{-3} and 322,000 OU·m^{-3}. The DBDs in these applications were exclusively laboratory plants with a small volume flow. Hence, enhanced SIE values of 9.2–187.5 kWh·1000 m^{-3} were used, in one case even 16,700 kWh·1000 m^{-3} [80–88].

Preis et al. (2013) [89] compiled an overview of existing plasma systems in the food industry for the reduction of odorous substances. Odor loads from other industrial applications were comprehensively investigated by Li et al. (2020) [12] at efficiencies of up to 98.7%.

2.3.3. Disinfection and Sterilization

Due to the current pandemic caused by SARS-CoV-2, the demand on disinfecting materials (e.g., protective masks), surfaces and room air has increased. Non-thermal plasmas are well suited for this purpose, as low operational temperature allows application with temperature sensitive materials and surfaces. A variety of so-called reference microorganisms, primarily bacteria, is used for evaluation of the disinfection performance. Microbial disinfection is generated by various mechanisms

Classical disinfection processes use a variety of so-called standard organisms, primarily bacteria. Disinfection is based on various mechanisms [16]:

(1) The reactive particles of the plasma chemically attack the microorganisms and damage the cell structure in a non-repairable extend [7,90–95].
(2) Electron bombardment creates pores in the cell walls, causing reactive particles to enter the cells directly and damage them [7,94,96–98].
(3) Ions can damage DNA and membrane proteins, impede functions or denature the cell membrane [7, 97].
(4) Plasmas form OH radicals and other particles in the presence of water molecules, which can lead to a pH shift within a cell. [99,100].
(5) The reactive particles also shift the redox potential and secondary toxins are formed [7]
(6) Electric charge can accumulate on the membrane surface.

Even since the outbreak of the pandemic, some research groups investigated the use of non-thermal plasmas for disinfection. Specifically, Lee et al., 2020 [101], investigated a DBD as a possibility for rapid disinfection of protective masks. Disinfection was primarily achieved by ozone, which is formed by the DBD. Whether plasma disinfection is really effective in deactivating or destroying viruses and in particular SARS-CoV-2 can hardly be proven due to complex cultivation by specific cell lines and handling of highly infectious viruses in comparison to bacteria [102]. Nevertheless, it can be assumed that non-thermal plasmas, which have been proven to have a disinfecting effect on bacteria, can also deactivate viruses.

2.3.4. VOC Abatement

VOCs play one of the most important roles in exhaust air purification, as they are emitted by multiple industries. The treatment of VOCs with DBD is considered and critically described in the reviews of Vandenbroucke et al. (2011) [44], Schiavon et al. (2017) [13], Chung et al. (2019) [103], Adelodun (2020) [104], Guo et al. (2020) [105] and Li et al. (2020) [12]. Although the feasibility of these processes has been demonstrated many times, the treatment of VOCs by NTP proves to be very difficult from an economical point of view, since the concentration of VOCs in the waste gas directly correlates with process' energy requirements. Therefore, the use of NTP processes seems to be either interesting for air pollutants having very low emission limits (e.g., cancerogenic compounds like benzene) or for VOC emission levels just above existing limits. A more advanced purification with higher energy input is generally possible.

2.3.5. Large-Scale Application

Various studies evaluated treatment of VOCs and other pollutants at commonly lab-scale conditions with low gas flows and high SIE values [12,16]. An overview of pilot plants with volume flows of 10 $m^3 \cdot h^{-1}$ or higher can be found in Dobslaw et al. (2018) [14] as well as in VDI guideline No. 2441 [106].

However, commercial and industrial implementation is very rare and reasons were described in detail [12]. Sum up, the reasons are the lack of adaptability to the state of gas, possible designs, operating costs, formation of byproducts and safety aspects.

3. Thermal Plasma

3.1. Designs and Operational Parameters

As mentioned above, plasma is a gas in which sufficient ionization processes take place by supplying energy, so that the free charges (ions and electrons) determine the properties of the gaseous phase. In contrast to the NTP processes of chapter 2, in thermal plasmas, the applied power is coupled into the system as heat by applying a direct voltage of up to 60 kV with over 95% of efficiency, whereby flame temperatures of up to 12,000 K, in water vapor supported systems of 14,000–22,000 K, can be achieved [107–110]. The high temperature of the process also allows the transformation of hardly convertible components like CF_4 or SF_6. The high reaction temperature also allows very short contact times.

The plasma temperature directly correlates with the coupled power and the gas volume flow to be treated and can be easily controlled via these two parameters. Correspondingly, low-volume but high-energy plasma gas flows can be used for treatment of waste gas. In addition to the resulting compact plant design, negative effects such as dilution of present concentrations, cooling effects as well as the formation of undesired byproducts can be efficiently reduced in this way, and the conversion efficiency can be further increased, although the concentration of the secondary products formed depends on a large number of parameters. Due to the high temperature level of the plasma, no carbon deposits occur as in combustion processes for PFCs, which can significantly increase process stability.

However, the efficiency of the process strongly correlates with the coupled power, the geometry of the plasma flame, the addition of additives, the mixing behavior of the waste gas during injection into the plasma zone and energy losses by cooling.

Under technical aspects, relevant plasma gases for the degradation of pollutants are helium, argon, nitrogen, steam, air and oxygen. Most frequently mixtures of argon and nitrogen are used [108,111,112]. In the case of noble gases and nitrogen, the addition of liquid water, water vapor or air is required for oxidative degradation of the pollutants. A detailed consideration of the effects of the various plasma gases on their behavior in the plasma with respect to conversion efficiency and the formation of secondary intermediates is given in a report by Dobslaw et al., 2019 [110]. Here, water vapor plasma proved to be the most efficient plasma form in the conversion of CF_4 (see also Section 6.1). More recently, H_2 and CO_2 have also become increasingly important as plasma gases for the production of synthesis gas [113–115].

The advantages of thermal plasmas are a high heat flow, high reaction temperatures, high energy densities, high concentrations of reactive components and thus high transformation efficiency with short contact times. Demand-oriented control, compact design and short start-up times are also possible. The high temperatures in the reaction chamber allow a rapid conversion even of components that are difficult to degrade. By controlling the temperature gradient in the reaction chamber, the coupled power and the addition of potential additives, both the transformation rate and the suppression of undesired byproducts can be accelerated. Furthermore, the demand on supplied gas and liquid is less extensive compared to combustion. The HCl or HF resulting from the treatment of CFCs, CHCs or PFCs can be easily eliminated by a subsequent alkaline scrubber.

On the other hand, there are disadvantages such as the formation of undesired byproducts, especially when oxygen is added as an additive (NOx, COF_2, CO, etc.), the need for cooling concepts

for the reaction chamber to prevent thermal damage to the torch, and a comparatively high electrical power requirement, which strongly depends on the plasma source used as well as the pollutant to be decomposed. Energetically optimized steam plasmas, for example, have a SIE value of approx. 2000–2200 kWh·1000 m^{-3} for the hardly degradable CF_4 [116–118].

3.2. Plasma Gases and Their Effects

As listed before, mixtures of argon and nitrogen are used as the most common technical plasma gases. In recent years, steam plasmas in particular have gained increasing relevance. Water can be offered to the plasma torch either as liquid or as externally generated steam. The advantages of water as a plasma gas compared to noble gases are, apart from clear economic aspects [119], the physical advantages. For example, the OH radicals produced have a high oxidative effect, and water vapor can provide higher energy densities due to its comparatively high c_p value than other plasma gases (see Figure 1).

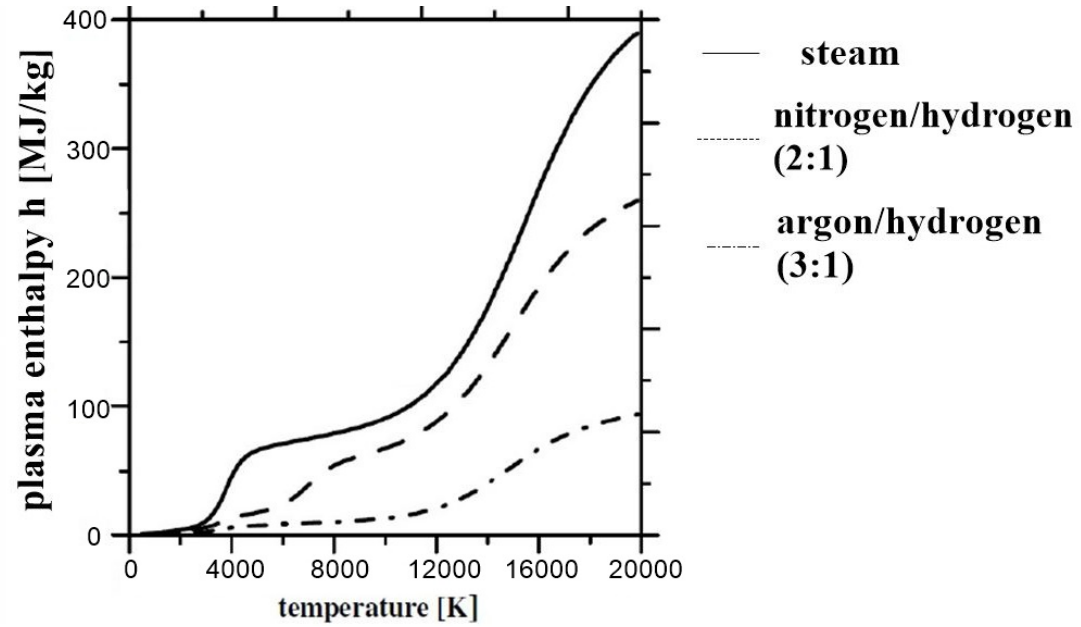

Figure 1. Comparison of the plasma energy densities of steam and mixtures of N_2 or Ar with H_2 as plasma gas as a function of the plasma flame temperature, based on Hrabovsky et al. (2011) [120].

Oxidative processes require the presence of oxygen molecules or atoms. An alternative to steam would therefore be oxygen as plasma gas, but pure oxygen leads to corrosive effects on electrodes and other components of the torch and reactor. As a consequence, the lifetime of such reactors is considerably reduced. Therefore, the use of water-supported plasmas is preferable. If steam is generated and fed in externally, it is advantageous to avoid cooling of the plasma flame by the evaporation enthalpy to be applied, thus avoiding negative effects on cleaning efficiency due to reduced temperatures.

Especially in the field of pyrolysis, Nishikawa et al. (2004) [121] have proven in experiments with charcoal that steam as plasma gas promotes the formation of a higher quality synthesis gas than argon or oxygen.

In the following, the different ways of introducing water are summarized. This is based on the usual system design, consisting of a plasma torch, a gas mixing chamber, a reaction chamber and a quench for gas cooling:

(1) Injection into the plasma chamber upflow the quench [116,122].
(2) Injection into the hot gas after quenching [116,122].
(3) Injection after quenching in the direction of the inner reactor wall [116,122].
(4) Transmission of the cold plasma gas through an upstream water tank [108,123].
(5) Passing the hot plasma gas through a downstream water tank [108,123].

The respective advantages and disadvantages are explained by Dobslaw et al. (2020) [16]. Common to all mentioned methods is that they work with liquid water. Commercially, variant 3 (injection in the direction of the inner reactor wall) is most frequently used, since it allows a long lifetime with low risk of deposits and, with regard to CF_4, a high degree of efficiency.

However, it is energetically more efficient to use water as steam. There are different process technologies to deal with this issue. Watanabe et al. [123–125] have developed a plasma source in which liquid water is vaporized in the anode area. Advantages of this technique are mainly the high-volume flow of up to 0.5 $L{\cdot}h^{-1}$ and the cooling of both the electrodes and the reaction chamber. However, it turned out to be a disadvantage that the liquid water flow led to a plasma cooling ($T_{max} < 3000$ K), and the evaporation of the water caused cavitation effects and damage of the torch. These negative effects led to a considerably reduced lifetime of less than 100 h.

Hrabovski et al. (2011) [120] tried to avoid the problem of corrosion by constructive adaptation. On the one hand, argon was introduced into the plasma chamber as a protective and plasma gas, and on the other hand, the inner walls were made of semi-permeable sintered metal and permeated by water. The steam produced by the heat was then introduced into the reaction chamber and provided sufficient cooling. In addition, the anode was designed as a rotating copper disc, which means that the discharge runs permanently along the edge, thus reducing local corrosion. Although the lifetime could be increased in this way, it requires an additional motor to drive the copper disc.

In a next step, Watanabe [126] used a hafnium electrode in a copper tube as cathode. A copper cylinder served as anode. The externally supplied water is vaporized by the waste heat at the anodes and fed into the plasma through the anode nozzle before the plasma gas escapes. With this process, an expensive shielding gas and an external vaporizer can be dispensed with. Disadvantages of this design are that no defined water vapor flow can be set, only a defined exhaust air flow is possible, strong corrosion effects occur and a high energy input is required.

Glocker et al. (2000) [127], on the other hand, works with external steam generation. The volume flow of the water vapor can thus be precisely adjusted and is passed by the cathode that is surrounded by argon, thus entering the plasma flame. The advantages of this process are the long lifetime of the cathode and the controllability of the steam flow. Disadvantages are the comparatively moderate lifetime of the anode, the expensive equipment for controlling the different gas flows and the necessary external cooling of the electrodes. This system configuration served as the basis for the further development described in later chapters.

3.3. Environmental Application

Thermal plasmas have been used in engineering applications since the 1980s. In the 1990s, they were also used for the first time in waste gas treatment. Since then, thermal plasmas have been successfully used for the treatment of gaseous emissions of VOCs such as acetone [128], decanol [129] and PCBs as well as PFCs (CF_4, C_2F_6, C_3F_8, C_4F_8, NF_3, SF_6, CHF_3, HFC-23, HFC-134a, HFC-32) [107,116,123,130–134]. Recently, thermal plasmas have also been used for the treatment of aqueous wastes [129,135] and for solids detoxification [126,136]. Due to the high energy demand described above, their use is restricted from an economic point of view in particular to exhaust air and waste streams that are very difficult to treat, such as the treatment of PFCs and CFCs.

Perfluorinated hydrocarbons such as CF_4, C_2F_6, C_3F_8, C_4F_8 as well as CHF_3, NF_3 and SF_6 occur as greenhouse relevant emissions in the semiconductor industry, in aluminum extraction as well as in the waste management industry and have also been used in the past in high-voltage equipment,

in magnesium die-casting as well as in the filling of car tires. More recently, PFC emissions from the electrolysis of rare earth fluoride/oxide systems such as neodymium and dysprosium have become increasingly important [137]. Total global emissions of CF_4, C_2F_6 and SF_6 in the two main sectors of the semiconductor industry and aluminum production were 42 Mt $CO_{2,eq}$·a^{-1} and 25 Mt $CO_{2,eq}$·a^{-1} (as of 2012) for CF_4 and C_2F_6, respectively, and 35 Mt $CO_{2,eq}$·a^{-1} of additional SF_6 in the semiconductor industry [137,138]. Further applications are surface cleaning and surface degreasing in the fields of electronics, electrical engineering and aerospace, high-voltage systems in heavy industry, filling gases in soundproof windows and car tires, magnesium die casting, various chemical syntheses in the chemical industry, as oxidizing agent for special fuels in the aerospace industry and the production of oscillating F_2 high-power lasers [139].

4. Design and Operational Parameter

4.1. NTP Plasma

Tests with NTP processes were carried out with an in-house developed DBD systems. Starting from a commercial product (Figure 2a), the short lifetime of reactive plasma components and the positive effect of catalytic adsorbers on cleaning efficiency were considered by developing a new housing with integrated PPC in the form of a drawer system (Figure 2b,c). As catalytic adsorbers, five different nanoscale clay minerals were tested according to Table 2. In pre-tests, these minerals were qualified with respect to their adsorption and desorption properties against selected waste gas components (methane 1 g·m^{-3}; n-butanol 0.1 g·m^{-3}; ammonia 0.1 g·m^{-3}). The test setup is shown schematically in Figure 3. A mixture of ammonia, n-butanol and methane at volume flows of 300, 500 and 700 m^3·h^{-1} was used as artificial waste gas in the NTP process. The geometrical parameters were previously described [31]. In parallel, a second system for spectroscopic analysis of the plasma discharge was developed by installing a polycarbonate window in the stack and in the front of the housing.

Table 2. Overview of the clay minerals used.

Manufacturer's Designation	Composition
GA 1	≥ 75% Bentonite ≤ 10% Muscovite ≤ 10% Cristobalite
GA 2	≥ 70% Halloysite ≤ 10% Nontronite ≤ 10% Hematite ≤ 10% Magnetite
GA 3	≥ 95% Halloysite ≤ 2% Alunite ≤ 2% Cristobalite
GA 4	≈ 60% Halloysite ≈ 40% Kaolinite
GA 5	≥ 85% Clinoptilolite ≤ 15% Quartz, cristobalite and muscovite in total

The flow profiles in the drawer-equipped NTP-PPC combination were simulated with the software Solidworks 2014, and the results of this simulation were incorporated into the design of a pilot plant as shown in Figures 4 and 5. This pilot plant, also an NTP-PPC combination, was built in a container design and equipped with a downstream installed drum filter with mineral adsorber GA2, an activated carbon coated honeycomb adsorber for ozone elimination and a bioscrubber with associated periphery built outside the container (bioscrubber only in phase I, see Figure 6). A cyclone and a commercial filter for the elimination of aerosols and dust were installed upstream. The selection of GA2 was based not only on the results of the pre-tests but also on the aspects of the commercial exploration grade of

the mining site and the political stability at the exploration site. With the installed ventilation capacity in the pilot plant, waste gas flows of up to 1000 $m^3 \cdot h^{-1}$ could be treated. Both laboratory and pilot plant could be operated in inline and bypass mode. In the interest of high process stability, the NTP was operated in bypass mode to exclude operational malfunctions due to high humidity or dust loads. The geometrical characteristics of this plant were previously described [14].

Experimental tests of this plant were carried out at three locations, whereby at location I, additional operating phases were simulated by adding various VOCs to the present waste gas. The central operating parameters ar4e summarized in Table 3.

Sampling points for gas analysis were available in the crude gas, after NTP stage, after mineral adsorber, after honeycomb and in the clean gas after the optional bioscrubber.

(**a**)

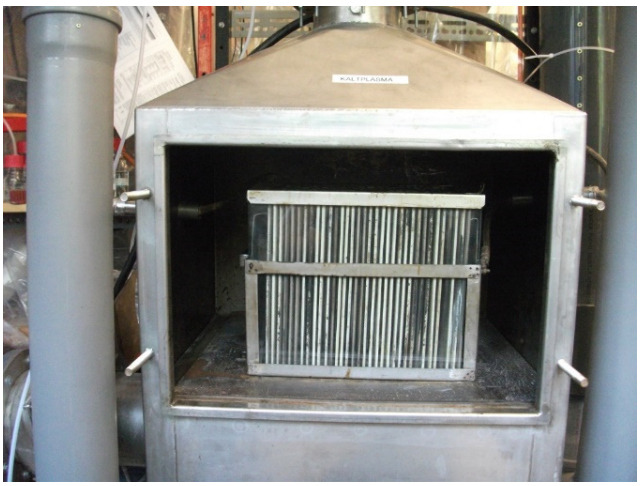

(**b**)

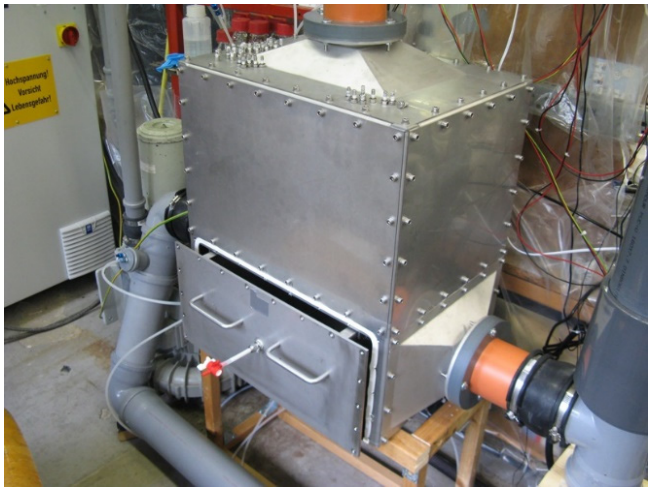

Figure 2. *Cont.*

(**c**)

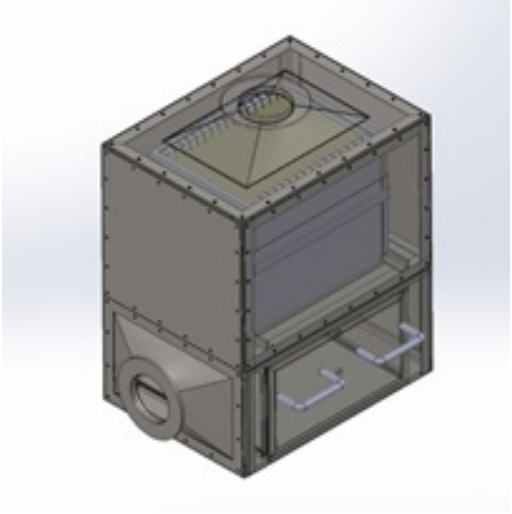

Figure 2. Design of the dielectric barrier discharge (DBD) systems without easy changeability between inflow and bypass operation (**a**) and the new housing with easy changeability and integrated drawer (**b**,**c**) [140].

Table 3. Overview of the operational phases of the pilot-scale system operating at a constant SIE of 2.1–2.2 kWh·1000 m^{-3} and a constant volume flow of 750 $m^3 \cdot h^{-1}$.

No. of Phase	Waste Gas Application	Location
I-I	Emissions sludge centrifuge	Wastewater treatment plant
I-II	Like I-I, spiked with styrene	
I-III	Like I-I, spiked with gasoline	
I-IV	Like I-I, spiked with 90 vol% styrene, 10 vol% ethanol	
I-V	Like I-I, spiked with n-butanol	
I-VI	Like I-I, spiked with 2-butoxyethanol	
II	Emissions of compost plant	Mechanical biological waste treatment plant
III	Emissions of sludge drying process	Organic waste digestion plant

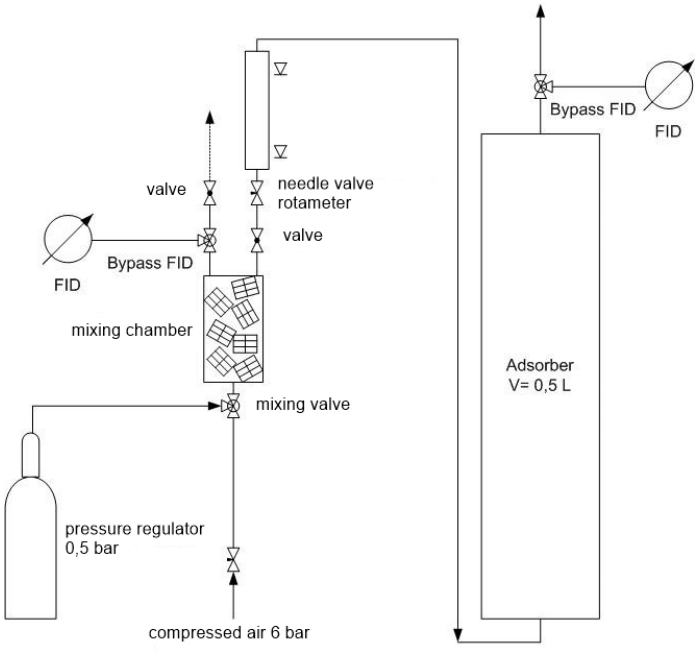

Figure 3. Setup for adsorption and desorption tests with artificial waste gases.

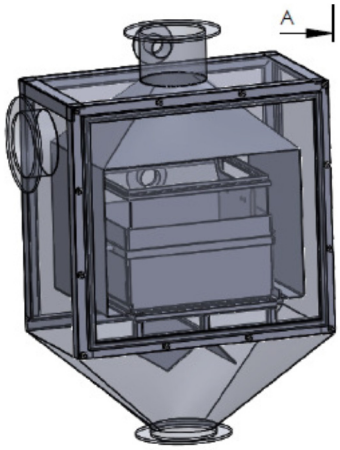

Figure 4. Cutaway drawing of the NTP stage for the pilot plant with optional inline or bypass operation mode up to 1000 m^3·h-1 of waste gas flow.



Figure 5. Interior view of the pilot plant in container scale showing pre-filtration (left), NTP with drum adsorber (center) and honeycomb adsorber with subsequent fan (right) and associated control technics and analytics.



Figure 6. Exterior view of the pilot plant in container scale showing the external bioscrubber (black column) and associated control and irrigation technology (within the green hut) installed at the wastewater treatment plant of the University of Stuttgart in Stuttgart-Büsnau.

4.2. Thermal Plasma

The evaluation of the thermal plasma was carried out at using an industrial-scale test system consisting of a gas supply, external vaporizer, power source, plasma torch, gas mixing chamber, reaction chamber, quench and an alkaline scrubber installed downstream. Figure 7 shows the installation in operation with an installed radiation-cooled reaction chamber (right) and supplemented gas analysis (left). The turnover of CF_4 as model pollutant in concentrations between 2790 ppm and up to 80,000 ppm at waste gas flows of 50–300 slm, at electrical power input of 12–20 kW, was tested using different plasma gases. As plasma gases N_2, O_2, air and water vapor were used. In addition, three reaction chamber geometries (waterfall film, radiation-cooled reaction chamber, recuperative reaction chamber) and two nozzle geometries (axially expanding nozzle, radially expanding Laval nozzle) were tested.



Figure 7. Indoor test system consisting of plasma torch, gas mixing chamber, reaction chamber and quench (right), an alkaline scrubber with pH control and corresponding dosage of 40 w% NaOH (center) and additional analytics (left).

5. Combined NTP/Bio Process for the Treatment of Complex Waste Gases

As described before, a combined system of NTP and subsequent biological treatment for energy-efficient treatment of complex waste gases such as those occurring in animal husbandry, animal meal drying, sewage sludge drying, waste composting, fermentation residue treatment and other industrial fields (50–100 organic components in total concentrations of some 100 mg C·m^{-3}, methane contents of 10–150 mg C·m^{-3} and odor concentrations of sometimes more than 20,000 OU·m^{-3}) should be achieved. The process of development can be subdivided into eight steps as follows:

1. Optical characterization of the plasma discharge as an indication of the formation of reactive components and the expected cleaning efficiency;
2. Development of a suitable catalytically active mineral adsorber;
3. Design and construction of a first prototype;
4. Testing of the prototype;
5. Flow simulation of the first prototype;
6. Development of a pilot plant for waste gas flows up to 1000 m^3·h^{-1},
7. Testing of the pilot plant;
8. Evaluation of experimental results and process stability with derivation of further development potentials.

5.1. Optical Characterization

The optical analysis of the discharge homogeneity of the plasma is an important indicator for the expected cleaning efficiency of the process, since only a homogeneous plasma discharge allows an optimized contact of the waste gas pollutants passing through with the generated reactive plasma components. The homogeneity of the plasma is influenced by the applied frequency of the AC voltage as well as by the applied current. The homogeneity of the plasma was therefore measured by varying these two parameters in the test system with spectroscopic access. Figure 8 shows the DBD-stack

(left) converted for spectroscopic access with the occurring discharge (right). The frequency of the discharge was varied in the range of 300–750 Hz, the current in the range of 7–19 A. Stable operating conditions with associated discharge characteristics are shown in Table 4. It can be seen that, as expected, the homogeneity and intensity of the plasma discharge increases with increasing current. Considering aspects of energy optimization of the system, it is interesting to note that a higher discharge homogeneity can be achieved at low frequencies. For further experiments, the operating condition at 11 A and 333 Hz was identified as the best set of parameters, since this is where the highest plasma homogeneity occurred. Additional experiments with variable gas flow at 11 A and 333 Hz did not show any effect on the homogeneity and stability of the plasma (data not shown).

Macro photos of the plates for a more detailed view of the discharges resulted in the situation shown in Figure 9. In the left figure, discharge channels are clearly visible showing a pronounced discharge foot at the ceramic barrier and a slender head at the electrode. Due to the use of a rough or structured ceramic material, the micro discharges occur preferably stationary at material elevations (right). These material elevations caused by the surface roughness represent fixed release points for the discharge, which is reflected in a higher light intensity at the discharge point.

Table 4. View on plasma homogeneity of some selected combinations of current and frequency [140].

Frequency [Hz] / **Power [A]**	**750**	**731**	**666**	**450**	**300**
7					
11					
15					
19					

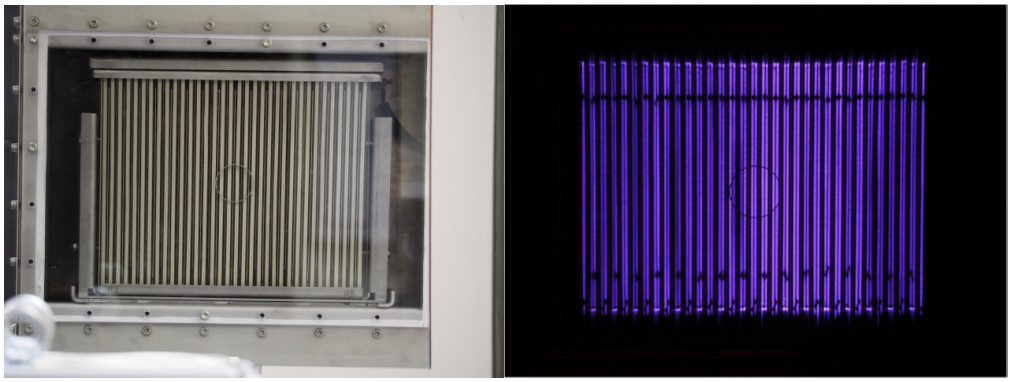

Figure 8. Test system for spectroscopic analyses with polcarbonate disk (**left**) and in operation mode (**right**) [140].

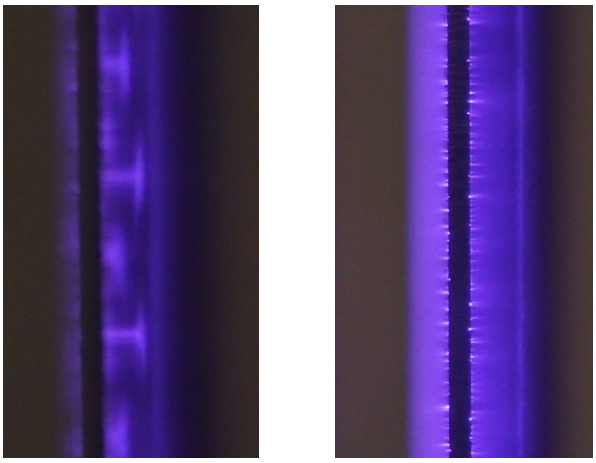

Figure 9. Individual plasma discharges, consisting of a thin discharge channel at the electrode and a wide base at the barrier (**left**). Dot-shaped starting points for small discharges on the surface of the barrier (**right**) [140].

Further spectroscopic analyses of the total discharges of the stack and the individual discharges as well were performed, showing no differences in the present discharge spectrum. Having a detailed look at the present electronic transitions, it was found that for DBD in air only the transition of nitrogen in the 2nd positive system could be observed (see Figure 10). In this excited level, nitrogen molecules have only a short lifetime and return to the basic level by light emissions. All other levels are excited to the ground state by impacts and thus non-radiative decay. Furthermore, a linearly increasing spectral absorption of ozone could be observed with increasing coupled power from 500 W on. Based on Figure 11, an ozone yield of 1 g ozone per 18.7 Wh of power input can be determined and, therefore, is in the upper range of the literature (1 g ozone per 20 Wh).

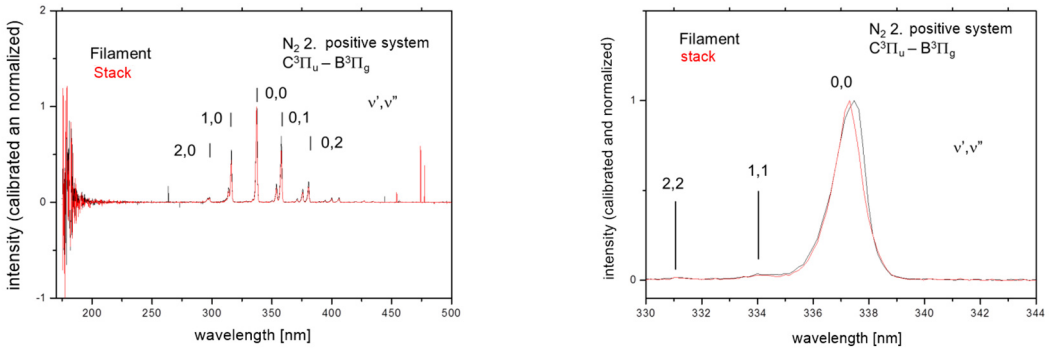

Figure 10. (**Left**) Emission spectrum of 175–500 nm showing emission of the 2nd positive system of the total discharge (red) and single filamentous discharge (blue). (**Right**) Enlargement of the transition (ν', ν'') = (0,0), i.e., $\Delta\nu = 0$. Both spectra show a nearly congruent course.

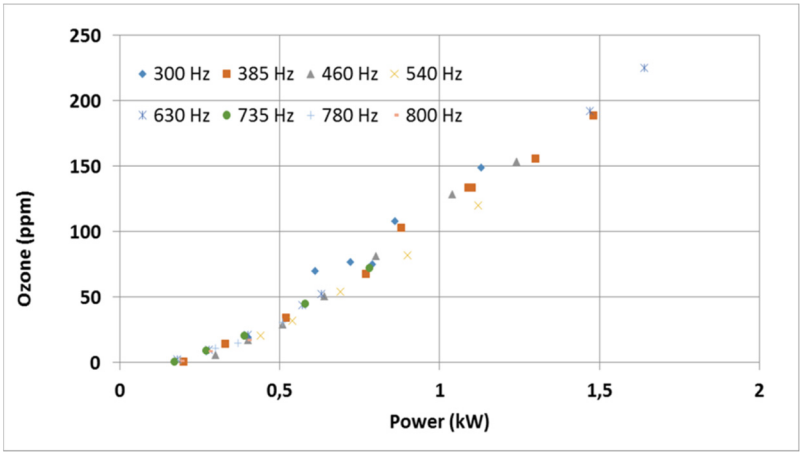

Figure 11. Ozone formation (ppm) as function of power input (kW) and frequency (Hz) [140].

5.2. Catalytically Active Mineral Adsorber

Multiple references in literature showed a significant increase in purification efficiency of the NTP in case of both adsorptive and catalytic effects of the installed PPC. In order to eliminate the potential risk of fire in the large-scale adsorber by glow discharge or induced flying sparks, nanoscale mineral materials were tested with regard to their adsorption capacity against methane, n-butanol and ammonia in realistic concentrations in continuous flow, which indirectly includes adsorption-relevant transport limitations. The results of these adsorption tests are shown in Table 5. Table 6 shows a ranking of the adsorbers used with regard to their adsorption capacity compared to the artificial waste gas components. Based on this ranking, the further use of GA 4 should be favored. However, since the degree of commercial exploration as well as the political stability at the exploration sites strongly regulated the availability and supply safety, the further tests were finally carried out with the material GA 2. The GA 1 material, which is also commercially readily available, was not pursued further, as exposure of this material to plasma and ammonia generated a white precipitate, which turned out to be ammonium sulfate with traces of pyrite and calcite and clogged the package of the adsorber by forming a top layer. Furthermore, formation of critical secondary intermediates like N_2O for GA 2 was lower than for GA 1.

Table 5. Adsorption characteristics of mineral adsorbers ($mg \cdot kg^{-1}$) at fixed crude gas levels ($g \cdot m^{-3}$).

	GA 1	GA 2	GA 3	GA 4	GA 5
Methane (1 $g \cdot m^{-3}$)	0.00274	0.00307	0.00342	0.0062	0.00477
n-Butanol (0.1 $g \cdot m^{-3}$)	4.86	2.6	4.35	3.29	1.21
Ammonia (0.1 $g \cdot m^{-3}$)	2.15	1.77	2.89	3.58	2.5

Table 6. Ranking of the mineral adsorbers tested based on the adsorption characteristics observed.

	Rank 1	Rank 2	Rank 3	Rank 4	Rank 5
Methane	GA 4	GA 5	GA 3	GA 2	GA 1
n-Butanol	GA 1	GA 3	GA 4	GA 5	GA 2
Ammonia	GA 4	GA 3	GA 5	GA 1	GA 2

5.3. Design, Construction and Efficiency of NTP-PPC System

GA 2 as selected material was further tested as PPC in combination with an upstream NTP in treatment of methane, n-butanol and ammonia as references. Performance was quantified by FID analysis (type 2010T, Testa GmbH, München, Germany) in the case of methane and n-butanol and by FTIR analysis for all three components (Antaris IGS, Thermo Fisher, Dreieich, Germany). The latter method also allowed the quantification of reaction products and secondary emissions.

The concentrations of the original pollutant and the reaction products are shown in Figure 12 (methane), Figure 13 (n-butanol) and Figure 14 (ammonia) for a fixed gas flow rate of 300 $m^3 \cdot h^{-1}$ (CH_4, NH_3) and 500 $m^3 \cdot h^{-1}$ (n-butanol), respectively.

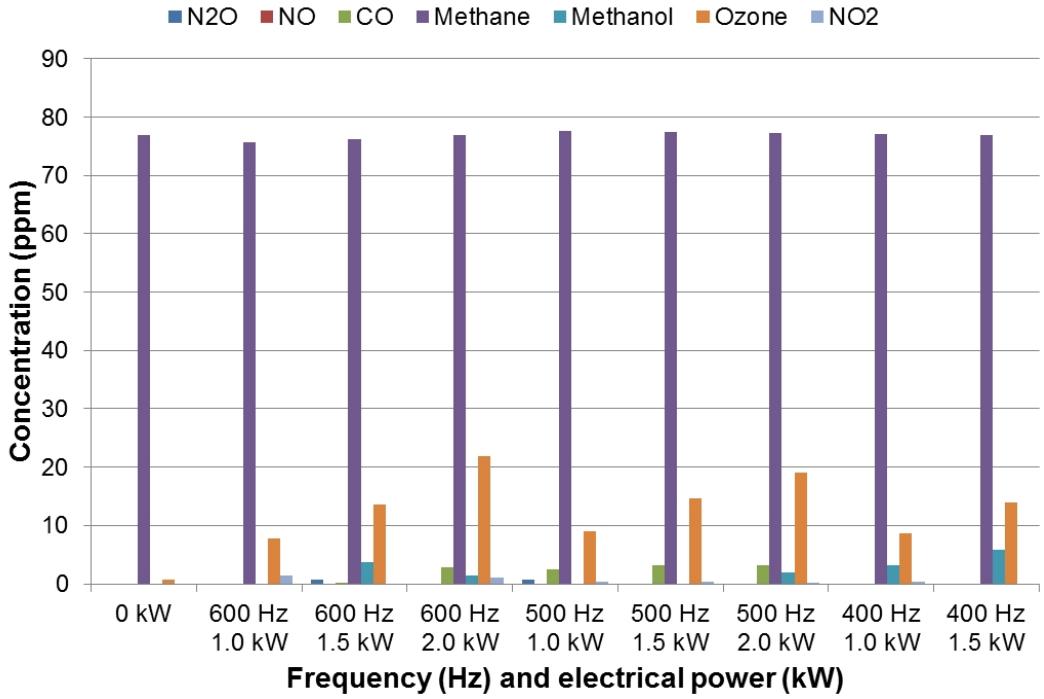

Figure 12. Concentration of methane as well as potential intermediates at different plasma operating conditions in combination with GA 2 at a gas flow of 300 $m^3 \cdot h^{-1}$.

As shown in Figure 12, no significant turnover of methane was observed under the current process conditions. Only in case of a power input of 1.5 kW and a frequency of 400 Hz higher levels of methanol occurred, indicating starting of methane conversion. However, the negligibly low efficiency at a SIE value of approx. 6.7 kWh·1000 m^{-3} indicates both an extremely questionable and non-energy-efficient conversion of methane, especially since the power consumption continues to rise with increasing methane concentrations and has to compete with incineration processes (SIE values approx. 16–21 kWh·1000 m^{-3}).

Energetically, the conversion of ammonia or n-butanol proves to be more favorable (see Figures 13 and 14). Efficiencies of 25–45% and 30–62% were achieved at concentrations of 49–69 ppm NH_3 and 50 ppm n-butanol and SIE values of 3.0–8.0 kWh·1000 m^{-3} and 3.3–6.7 kWh·1000 m^{-3}, respectively. However, performance remained well below expectations.

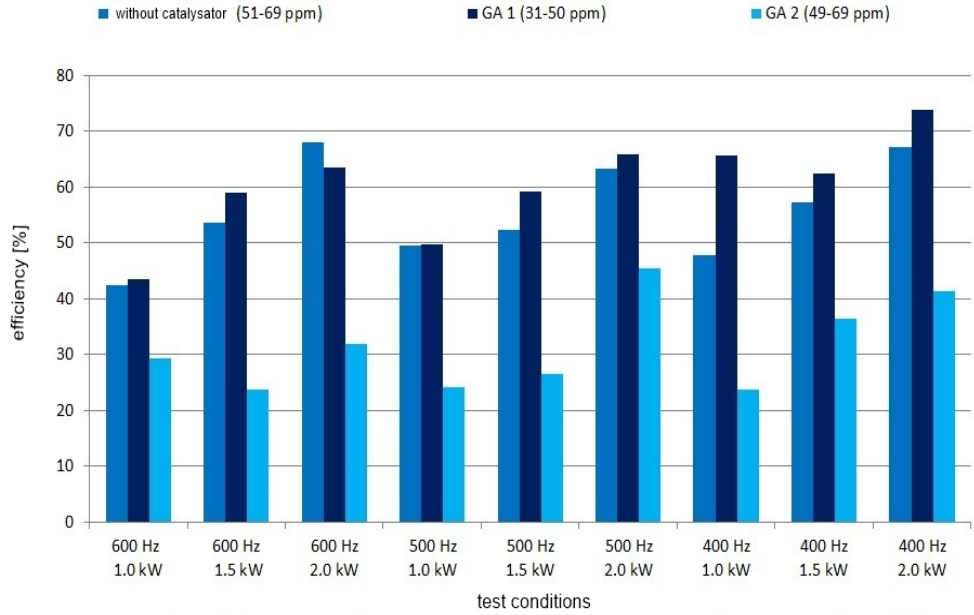

SIE (kWh/1000 $m^3 \cdot h^{-1}$)	3.7	3.5	3.0	5.8	5.2	4.7	8.1	6.8	6.5	3.7	3.5	3.1	5.7	5.3	4.7	8.0	6.8	6.4	3.7	3.5	3.2	5.7	5.3	4.8	8.0	7.0	6.1
EC (kWh/kg NH_3)	213.5	295.6	215.3	215.0	259.7	432.5	284.7	311.6	448.5	201.0	305.5	281.9	215.3	277.0	428.8	248.1	302.6	307.9	209.3	232.4	333.6	192.5	307.9	328.8	235.3	277.4	322.0

Figure 13. Comparison of the cleaning efficiency of the mineral adsorbers GA 1 and GA 2 versus performance without PPC in case of ammonia at a gas flow of 300 $m^3 \cdot h^{-1}$ in bypass operation mode. Additionally, the corresponding SIE and EC values are presented.

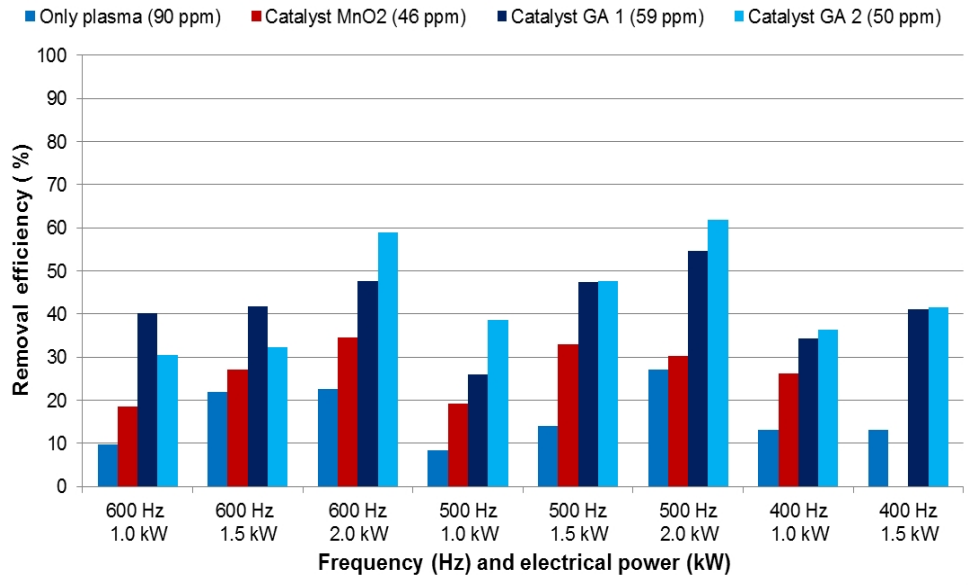

SIE (kWh·1000 m^{-3})	3.3			5.0			6.7			3.3			5.0			6.7			3.3			5.0		
EC (kWh·g BuOH^{-1})	68.7	71.2	25.5	39.5	45.8	72.5	36.8	56.3	59.6	75.9	43.1	41.1	80.6	68.7	39.5	31.3	72.0	59.9	32.4	38.2	49.4	86.8	37.6	39.1	50.8	50.3	29.9	33.2	76.2	k.A.	37.4	43.7

Figure 14. Comparison of the cleaning efficiency of the mineral adsorbers GA 1 and GA 2 versus performance without PPC and MnO_2 as reference catalyst in case of n-butanol at a gas flow of 500 $m^3 \cdot h^{-1}$ in bypass operation mode. Additionally, the corresponding SIE and EC values are presented. Bars are mean values of 72 individual measurements with a relative measurement deviation within the series of less than 2.5%, equivalent to less than 1.5% in total.

5.4. Flow Simulation of the NTP-PPC Process

According to the low performance levels, the flow profiles in the plasma stage as well as in the adsorber drawer were simulated for both inline and bypass operation at gas flows of 300, 500, and 700 $m^3 \cdot h^{-1}$ in inline operation and for the same gas flows with an additional auxiliary air flow of 65 $m^3 \cdot h^{-1}$ in bypass mode. Figure 15 shows the situation in bypass operation mode with 300 $m^3 \cdot h^{-1}$ of waste air and 65 $m^3 \cdot h^{-1}$ of auxiliary air. Here, the waste air is supplied from the left, while the auxiliary air is supplied from the top. The simulation profiles show on the one hand that the waste air does not flow through the bed but flows quantitatively around the adsorber package via the small gaps on both sides between the respective guide rail and the drawer, so that the adsorber performs neither as catalyst nor as adsorber. On the other hand, it can be seen that even with this small waste air flow, the pressure loss distribution in the system leads to a backflow of the waste gas into the stack, where it causes strong turbulence above the stack. The backflow of the waste gas leads to a second contact with the plasma stage, which probably leads to the higher efficiency compared to the sole plasma operation mode.

In addition, it was found that the amount of mineral adsorber as used in the drawer model is unsuitable for industrial use, as the drawer system would be unmanageable with waste gas flows of 1000 $m^3 \cdot h^{-1}$ or higher. The advantage of the very short gas flow distance between plasma module and adsorber therefore had to be dropped as well.

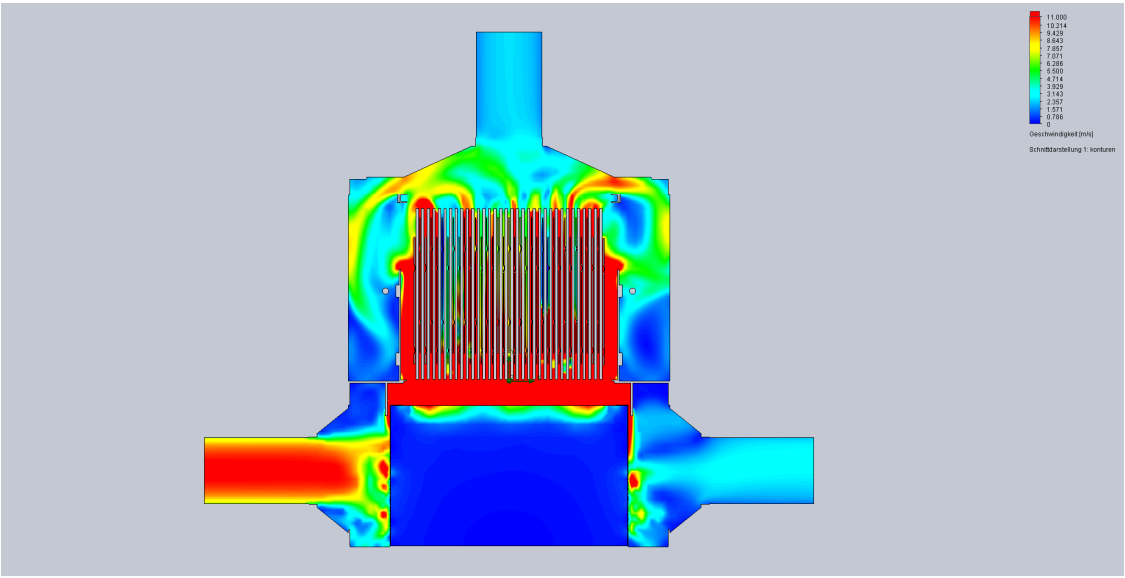

Figure 15. Flow simulation of the combined non-thermal plasma (NTP)- post-plasma catalysis (PPC) in inline operation mode with 300 $m^3 \cdot h^{-1}$ of waste gas and 65 $m^3 \cdot h^{-1}$ of auxiliary gas in side view [31].

5.5. Design, Construction and Efficiency of the Pilot-Scale NTP-PPC-Bioscrubber System

In view of the disadvantages mentioned above, a further concept was developed, consisting of NTP and a drum containing the mineral adsorber in downstream. Through separation of both stages, possible backflow effects were excluded, and mixing of the waste gas with auxiliary gas during bypass operation was improved in the NTP stage built as case-in-case model. Side flows were further reduced by reducing distances and installing seals. This improved housing also allows easy switching between inline and bypass operation. Flow simulations of the NTP housing underlined the improved gas mixing and were previously described in detail [31]. The plant was operated during three operational phases according to three different waste gas sources according to previous Table 3 and extended by a bioscrubber as final cleaning stage during the first operating period in order to eliminate the partially oxidized components in an energy-efficient biodegradative way [31]. The process time of this first

phase is subdivided into six stages, which are characterized by an artificial addition of VOCs to the original emissions from the sludge centrifugation.

In stage 1, crude gas concentrations of 30–50 mg C·m^{-3} were measured. Methane levels ranged between 30–110 ppm, and ammonia was about 0.2 ppm on average. According to the poor results of methane conversion during the pre-tests with the drawer model, little or no methane degradation could be detected. However, removal efficiencies of 100% and 78% were achieved in the degradation of ammonia and odor, respectively.

After 12 days, the crude gas was spiked with 9–15 mg C·m^{-3} styrene (stage 2), because concentration levels of VOCs in the crude gas from the sludge centrifugation were too low. The styrene was almost completely removed from the waste gas. Benzaldehyde, heptanal and hexanal were detected as more hydrophilic conversion products.

An addition of super gasoline increased the total carbon levels to up to 300 mg C·m^{-3} in maximum (stage 3). In contrast, VOC levels in the clean gas after DBE were less than 40 mg C·m^{-3}.

In a further step, the system was charged with a mixture of 90% styrene and 10% ethanol (stage 4), thus achieving an average concentration of 50–70 mg C·m^{-3} and a maximum level of 350 mg C·m^{-3} in the crude gas. In the clean gas levels of 0–20 mg C·m^{-3} were measured during this test series.

Since the laboratory tests showed quite good results in the degradation of n-butanol, n-butanol was also added to the crude gas in step 5. With an addition of 40–60 mg C·m^{-3} n-butanol, degradation efficiencies of up to 60% and, therefore, about 30% higher than during laboratory pre-tests (efficiency was 30% in maximum) were achieved. Measurements after the biological stage even showed degradation rates of 93–100%.

Finally, 2-butoxyethanol was added in step 6. Due to its low vapor pressure, only low C loads could be evaporated, which meant that only increases in gas concentrations of 15–20 mg C·m^{-3} were achieved. Accordingly, an average of 10 mg C·m^{-3} of the carbon concentration could be eliminated by plasma treatment.

Results of the operational periods II and III were previously described in detail [14]. Nevertheless, some additional aspects of operation during period III (treatment of dryer waste gas) should be pointed out. The combined system without bioscrubber was installed for several months at the solid waste fermentation plant in Leonberg to treat waste gas emissions of the belt dryer for drying of the fermentation residues of the fermentation process of solid wastes in a bypass process. The performance of the system was evaluated by continuously operating FID and FTIR analyses and discontinuously operating olfactometric and GC-MS analyses. However, latter tests were stopped after a short time due to the low loads of emissions. Unfortunately, long-term continuous analysis of the process was not possible, because the plant had to struggle with different technical difficulties. To solve these problems, the control system had to be partially deactivated, which, however, prevented the plasma from being ignited automatically. Due to the wet and cold weather in the winter months, the relatively high humidity of the fresh air supply led to recurring system malfunctions. In addition, at the end of the test period, there was a longer shutdown of the plant, as a fire broke out inside the fermentation plant. An exemplary section of the analytical data is presented in Figure 16.

The VOC removal efficiency during the time period of Figure 16 ranged within 10–50%, in individual cases, 100% was also achieved. While the removal of VOCs as total carbon and as various individual components could not provide satisfactory results, which is partly due to the discontinuous test procedure, the olfactometric investigations showed a reproducible positive effect of the plasma-supported treatment of the waste gas. Permanent removal of odor by more than 95% was achieved.

In a subsequent phase IV, the sole NTP stage was connected downstream of a biotrickling filter for the treatment of styrene emissions in order to efficiently sterilize the clean gas. This study was previously described by Helbich et al. (2020) [141]. In summary, a disinfection of more than 3 log units was achieved. This finding also underlines the possibility of using NTP processes for disinfection.

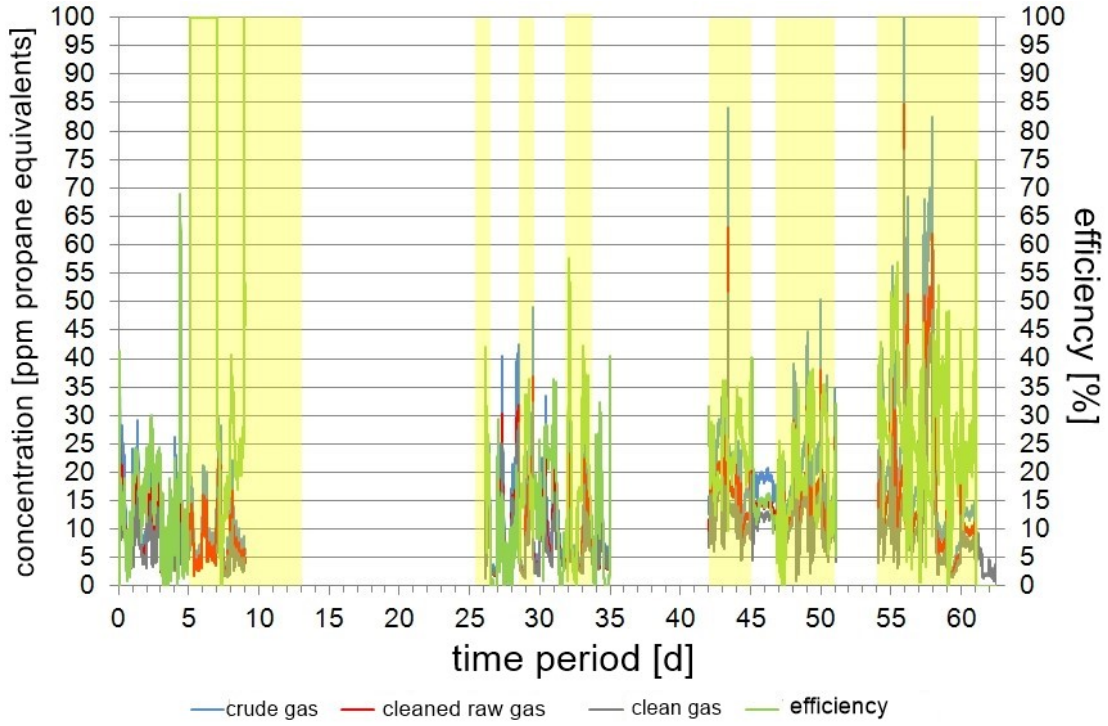

Figure 16. Course of VOC levels in crude and clean gas (after activated carbon filter) in the belt dryer waste gas of the Leonberg solid waste fermentation plant. NTP is turned on during yellow shaded time periods.

5.6. Experimental Evaluation, Costs and Development Potentials

The difficulties that have already been described in practical operation show that there is still room for improvement in various areas. The necessity of bypass operation of the NTP stage in case of humid or dust-laden waste gas has a particular effect on the technical performance. While an efficient dust removal can be achieved by pre-treatment stages, a reduction of the air humidity is only possible either by drying, intermediate heating or by adding dry air. In view of the high waste gas flows, all approaches are associated with high costs, which is why the loss of short-living reactive components out of the plasma discharge must be accepted in order to achieve a cost-efficient reduction of the waste gas humidity by a cost-effective addition of fresh air. Fresh air is led directly through the plasma and serves as a carrier gas for the reactive products to mix them into the waste gas of large volume flows. Besides the humidity itself, a rising water content of the barrier sheets at high humidity process conditions has a negative effect on the process stability, since the dielectric constant of the sheet can decrease by several log levels, leading to increased flashover formation. Additionally, a residual structuring of the plates shows a significant influence on the homogeneity of the plasma discharge. Current in-house research therefore focuses on even, moisture-repellent barriers with preferably catalytic and adsorptive properties and lower weight than the current plates in order to achieve not only a simplified handling but also lower manufacturing costs. Especially the barrier plates cause a high proportion of the constructive costs. If the approach of the process combination of NTP-PPC-bioscrubber is successfully pursued, i.e., the NTP stage is used for partial oxidation of the mostly lipophilic waste gas components and the same is mineralized energy-efficiently by a compact biological process in downstream, the process combination already represents an interesting process alternative even with the current constructive costs for the barriers. In a study by Dobslaw et al. (2017) [31] a comparative calculation with an sole NTP-PPC process has already been carried out based on calculations of Martin et al. (2008) [142]. Extrapolated to a waste gas flow of 20,000 $m^3 \cdot h^{-1}$, the cost advantage of the combination with biological aftertreatment could be estimated at EUR 71,100 in constructive costs and in the range of EUR 37,450–150,250 in operating costs per year, equivalent

to a cost reduction of specific constructive costs of 3.56 €·h·m^{-3} and specific operating costs of EUR 0.24–0.94·1000 m^{-3}. If the development of new barriers succeeds, the constructive costs can be further reduced by a medium five-figure amount, and the operating costs can be reduced by approx. 20% through the inline use of the NTP stage.

5.7. Ecological Aspects and Sustainability

In addition to the economic saving potential of NTP processes compared to conventional combustion processes, NTP processes also have a clear advantage from a sustainability perspective. In the case of the NTP processes, CO_2 emissions according to Table 7 result quantitatively from the provision of the electric current for the generation of the plasma discharge (67.0%), while in the case of combustion CO_2, emissions are produced both by the combustion of natural gas as fuel (42.8%) and by the formation of nitrous oxide as secondary pollutant (41.6%). A direct quantitative comparison of the two processes shows that the NTP process has a savings potential of almost 40 t CO_2,eq·a^{-1} per 1000 m^3·h^{-1} of gas flow or 67.3% compared to the conventional combustion process.

Table 7. Balancing of emissions of CO_2, CH_4 and N_2O as greenhouse gases for combustion and NTP processes for treatment of a gas flow of 1000 m^3·h^{-1} for 8000 h·a^{-1}. Data based on CO_2 emissions of the German energy mix in 2019 (0.401 kg CO_2·kWh^{-1}). * analytical data of the authors; ** experience values for combustion.

Parameter	Incineration		Non-Thermal Plasma	
	Quantity	**in $CO_{2,eq}$**	**Quantity**	**in $CO_{2,eq}$**
Natural gas	12,729.5 m^3·a^{-1}	25,003 kg·a^{-1}	0 m^3·a^{-1}	0 kg·a^{-1}
Methane emissions	24.0 kg·a^{-1} (3 mg C·m^{-3} **)	504 kg·a^{-1}	3.31 kg·a^{-1} (0.58 ppm *)	69.6 kg·a^{-1}
Energy demand fan	17.6 MWh·a^{-1} (Δp = 5000 Pa)	7040 kg·a^{-1}	8.8 MWh·a^{-1} (Δp = 2250 Pa)	3520 kg·a^{-1}
Energy demand compressor	4 MWh·a^{-1} (P = 0.5 kW)	1600 kg·a^{-1}	0 kWh	0 kg·a^{-1}
Energy demand DBD	0 kWh	0 kg·a^{-1}	32 MWh·a^{-1} (4 kWh·1000 m^{-3})	12,800 kg·a^{-1}
N_2O formation	78.5 kg·a^{-1} (5 ppm **)	24,330 kg·a^{-1}	8.8 kg·a^{-1} (0.57 ppm *)	2728 kg·a^{-1}
Sum		**58,477 kg·a^{-1}**		**19,118 kg·a^{-1}**
Reduction potential	**0 kg·a^{-1}**		**39,359 kg·a^{-1} or 67.3%**	

6. Optimization of Thermal Plasma Processes

According to the state of the art as described above, thermal plasmas have four major problems:

1. Insufficient efficiency due to heat losses;
2. Insufficient efficiency at high waste gas flows and thus limited SIE values;
3. Quality and quantity of byproducts;
4. High losses of coupled power by high heat losses.

In order to meet these problems, test series with different reactor geometries and plasma gases were carried out based on the water vapor plasma developed by Glocker et al. [127] with the objective that the reaction temperature in the plasma zone should be kept above 2500 K for large plasma volumes.

6.1. Effect of Geometry and Plasma Gases

Within these tests, two fundamentally different reaction chamber geometries (waterfall film, radiation-cooled chamber), two nozzle geometries (axially expanding nozzle or radially expanding Laval nozzle) as well as four different plasma gases (H_2O, N2, O_2, air) were initially investigated, and the water vapor plasma was selected as the most promising plasma gas and the radiation-cooled reactor geometry as the preferred geometry. Test series on the influence of the volume flows of waste

gas, plasma gas, coupled electrical power, concentration of CF_4 and nozzle geometries showed a strongly differentiating result.

In the case of the plasma gases, O_2 and air, the formation of high concentrations of NOx was shown, which are responsible for the formation of ground-level ozone and acid rain due to their toxicity and relevance for acid rain. Their formation is also of high relevance in the technical system, since due to their acidic character, the consumption of caustic solution in the downstream scrubber rose sharply, thus worsening the economic balance. A corresponding configuration was no longer considered.

Furthermore, the falling film system showed a significantly higher heat loss to the water phase compared to the radiation-cooled approach, which was indirectly shown by a lower cleaning performance compared to CF_4 under comparable conditions. This effect is illustrated in Table 8, which provides a summary of the efficiencies as a function of the injected CF_4 concentrations for the existing configuration of the steam plasma, the new development with a perforated inner shell and the falling film systems based on H_2O or N_2 plasma. The direct comparison between nitrogen and water vapor plasma in the falling film shows a significantly higher efficiency of the water vapor plasma based on the differences in efficiency. The comparison of the two basic reaction chamber geometries shows an advantage of the radiation-cooled system, which resulted in a significant improvement of the CF_4 conversion compared to the previous system. In the case of the illustrated waste gas situation of 100 slm, the negative effect of decreasing efficiency caused by cooling power is not yet noticeable in the case of the falling film system, but is already clearly evident at 150 slm as previously shown [118]. In case of missing data within the table no test results were available. The CF_4 turnover as well as the concentration of occurring secondary metabolites were analytically evaluated by a combination of FTIR (detection of inert gases, CF_4 as well as short-chain organic transformation products) and GC-MS (detection of CF_4 and unknown organic transformation products).

To investigate the effect of the nozzle geometry on the plasma geometry, the geometry of the plasma discharge was directly analyzed at the separated plasma torch, and differences in operational parameters were evaluated by imaging techniques.

The radiation-cooled configuration of the predecessor model was convincing and was therefore used as the basic model for further development (Figure 17).

Table 8. Efficiency overview of different systems—original system, optimized system and commercially available water film system (with water and nitrogen as plasma gases) at 100 slm as a function of CF_4 concentration at 20 kW of input power.

	Original System	**Prototype**	**Water Film with H_2O Plasma**	**Water Film with N_2 Plasma**
0	0%	0%	0%	0%
2790 ppm	-	100%	-	-
5500 ppm	85.1%	100%	95.8%	87.3%
11,000 ppm	92.3%	99.9%	-	85.3%
22,000 ppm	87.7%	99.8%	-	80.9%
40,000 ppm	89.2%	99.3%	-	-

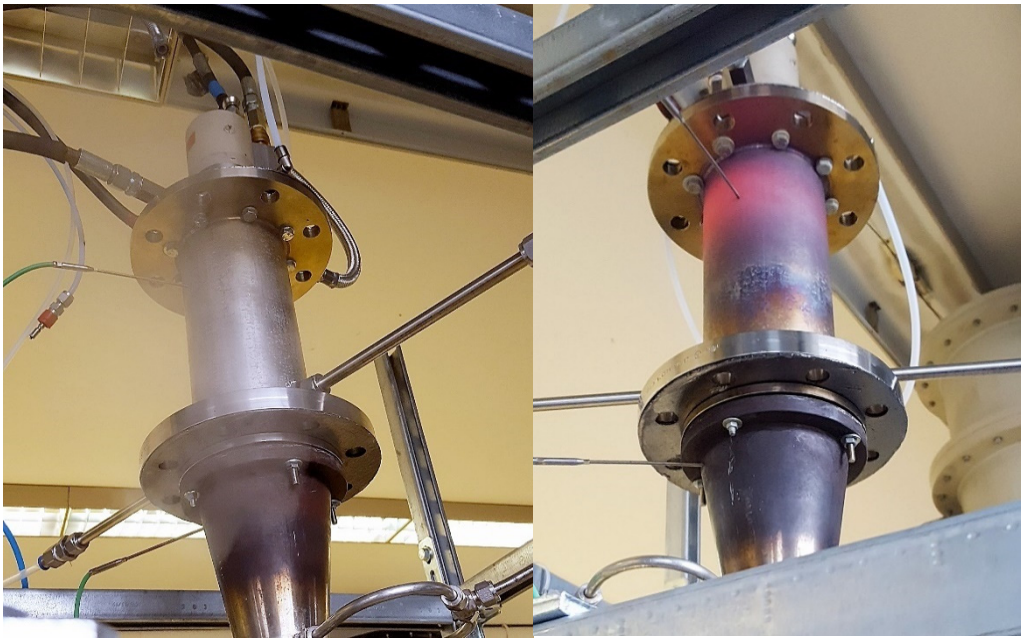

Figure 17. Prototype of the radiation cooled plasma system during start-up (**left**) and permanent operation (**right**).

6.2. Flow Simulation of the Reaction Chamber

Solving the problem of optimal injection and mixing of the waste gas into the plasma zone of the reaction chamber, flow and heat simulations with the simulation software Ansys Fluent 2018 were carried out using a system of a tube-in-tube reactor with a perforated inner wall. For the structural design of the reaction chamber, simulations with variation of the plasma gas flow, waste gas flow as well as the coupled electrical power were carried out. Exemplarily results of these simulations are presented in Figure 18a showing the original system of the radiation-cooled reactor at a power input of 10 kW, a waste air flow of 150 slm and a plasma gas flow of 30 slm, whereby the waste gas is injected directly at the torch head. The model shows a good mixing behavior due to an impingement jet of plasma gas and waste gas in the area of the entrance of the reaction chamber. However, a distinct temperature profile within the reactor also occurs, which indicates a resulting temperature of less than 2400 K shortly after injection of the waste gas. The minimum conversion temperature of CF_4 (approx. 2500 K) described in the literature is thus already undercut in the reaction chamber head, so that a power input of 10 kW is too low for successful conversion of CF_4 (corresponds to SIE = 1100 kWh·1000 m^{-3}). In total, a temperature drop of approx. 600 K occurs over the length of the reaction chamber.

Figure 18b,c shows the temperature and turbulence profiles for the tube-in-tube model at the same gas flows (150 slm of CF_4-containing waste gas; 50 slm steam; 20 kW power input, corresponding to 2222 kWh·1000 m^{-3}) injecting the waste gas via the perforations. The previously observed impact jet no longer occurs due to the lack of injection via the nozzles in the mixing plate between the burner and the reaction chamber. The simulation results in the perforation plane show for the temperature distribution a strong cooling plume in the area of the perforation, which continues upwards towards the reactor head. On the other hand, a strong temperature rise to approx. 2800–3000 K occurs just below the perforation over the entire cross-sectional area of the reactor. This is due to the principle of jet injection. The high exit velocity of the plasma gas initiates a suction effect for the air flowing in at the wall, which causes cool waste gas to be torn upwards. The waste gas is thus sucked into the center of the plasma flame. At the same time, the "negative" temperature profile leads to a strong radial outflow of the plasma gas towards the reactor wall below the injection zone, which can be further enhanced by using the radially expanding Laval nozzle. Since the temperature profile in the present case is very high overall, an efficient CF_4 treatment seems possible. The gas velocities in the center of

the reactor are very high and support explanations given above. The described velocity profile is also shown in Figure 18c. The simulation results indicate that due to the reduced radiation cooling of the reactor outer wall, the gas temperature inside the combustion chamber can be kept above 2300 K even at gas flows of 300 slm (Figure 18d).

(**a**)

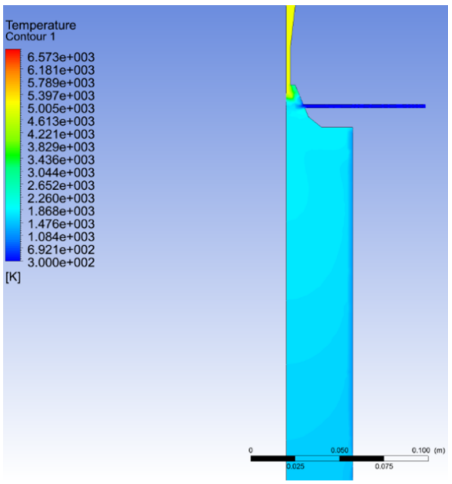

(**b**)

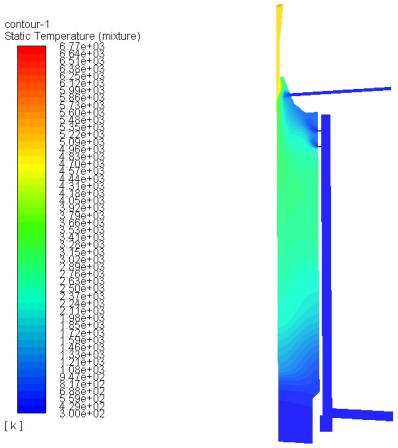

(**c**)

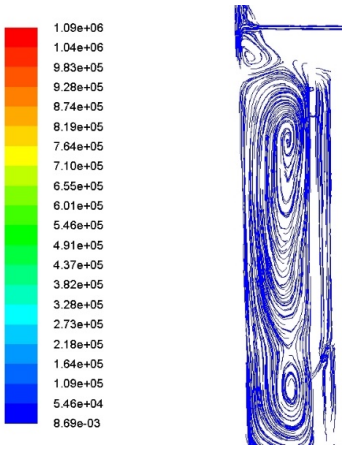

Figure 18. *Cont.*

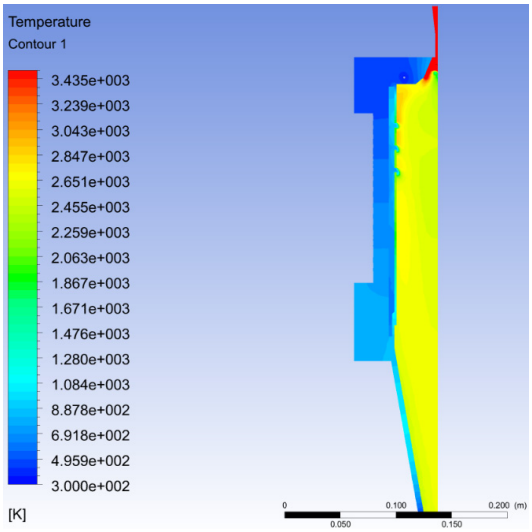

(**d**)

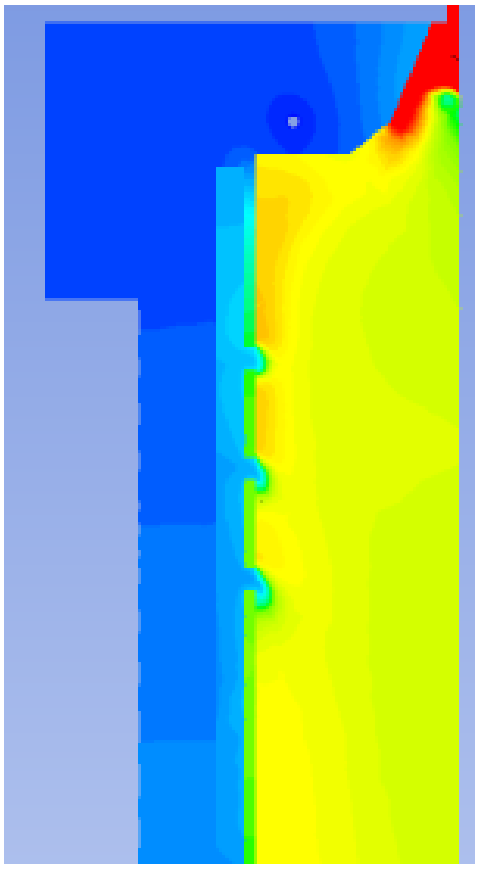

Figure 18. (**a**) Temperature simulation of the original system at gas flows of 150 slm and 30 slm and 10 kW of power input; (**b**) temperature simulation of the system with perforated inner wall at 150 slm and 50 slm and 20 kW of power input; (**c**) flow simulations at conditions of (**b**); (**d**) temperature simulation like (**b**) but at 300 slm of waste gas.

This improved temperature profile within the reaction chamber could be confirmed in practical tests on the prototype (see Table 9). It can be seen that the prototype achieved higher efficiency than the predecessor model across all concentrations. In comparison to the commercial model, the efficiencies are significantly higher, too, with almost complete turnover of CF_4.

Table 9. Comparison of the transformation efficiency of CF_4 in the previous radiation-cooled combustion chamber compared to the innovation with integrated heat recovery for volume flows of 150 slm and 300 slm of waste gas with concentrations of 2790–22,000 ppm of CF_4 at a power input of 20 kW.

	Conventional System		Prototype	
Concentration (ppm)	**150 slm**	**300 slm**	**150 slm**	**300 slm**
2790	94.4%	68.7%	100.0%	91.7%
5500	95.5%	65.9%	99.9%	92.9%
8250	95.0%	63.5%	100.0%	87.4%
11,000	94.6%	67.0%	100.0%	86.6%
14,000	-	-	-	87.7%
22,000	94.5%	-	100.0%	-

6.3. Ecological Evaluation of Thermal Plasmas

The present analytical data show a very high demand on electrical energy (SIE = 1100–2200 kWh·1000 m^{-3}) compared to other waste gas treatment processes, which initially gives rise to strong doubts about the sustainability of these processes.

However, due to the high chemical stability, the high vapor pressure and the insolubility of CF_4 in water, conventional waste gas treatment processes are not applicable. Only post-combustion processes are used as an alternative, but these are characterized by a very low efficiency of 16–52% [143,144]. Due to this low efficiency and the high global warming potential of CF_4 (factor 7349 compared to CO_2), this impression is completely put into perspective, as shown in Table 10.

When treating emissions with a high global warming potential, it is therefore essential to achieve very high cleaning efficiencies, since the CO_2 fingerprint of these components is many times higher than the CO_2 emissions from energy generation. Nevertheless, energy-efficient methods represent a clear competitive advantage, especially in this application.

Table 10. Balancing of emissions of CO_2, CH_4 and N_2O as greenhouse gases for combustion and NTP processes for treatment of a gas flow of 1000 $m^3 \cdot h^{-1}$ for 8000 $h \cdot a^{-1}$. Data based on CO_2 emissions of the German energy mix in 2019 (0.401 kg $CO_2 \cdot kWh^{-1}$). * Analytical data of the authors. ** Experience values for combustion. *** Calculated value based on a concentration of 10 $mg \cdot L^{-1}$ of ammonia as fertilizer in the swamp phase at pH 7.8 and ammonium/ammonia distribution of Kollbach [145].

Parameter	**Incineration**		**Thermal Plasma**	
	Quantity	**in $CO_{2,eq}$**	**Quantity**	**in $CO_{2,eq}$**
Natural gas	12,729.5 $m^3 \cdot a^{-1}$	25,003 $kg \cdot a^{-1}$	0 $m^3 \cdot a^{-1}$	0 $kg \cdot a^{-1}$
Methane emissions	24.0 $kg \cdot a^{-1}$ (3 mg $C \cdot m^{-3}$ **)	504 $kg \cdot a^{-1}$	0 $kg \cdot a^{-1}$	0 $kg \cdot a^{-1}$
Energy demand fan	17.6 $MWh \cdot a^{-1}$ (Δp = 5000 Pa)	7040 $kg \cdot a^{-1}$	17.6 $MWh \cdot a^{-1}$ (Δp = 5000 Pa)	7040 $kg \cdot a^{-1}$
Energy demand compressor	4 $MWh \cdot a^{-1}$ (P = 0.5 kW)	1600 $kg \cdot a^{-1}$	0 kWh	0 $kg \cdot a^{-1}$
Energy demand DBD	0 kWh	0 $kg \cdot a^{-1}$	0 $MWh \cdot a^{-1}$	0 $kg \cdot a^{-1}$
Energy demand vaporizer	0 kWh	0 $kg \cdot a^{-1}$	381.6 MWh	153,000 $kg \cdot a^{-1}$
Energy demand torch	0 kWh	0 $kg \cdot a^{-1}$	8888 MWh (P = 1111 kW)	3,564,000 $kg \cdot a^{-1}$
Efficiency	Concentration CF_4 [ppm] 16–52%		22,000 99.8% (*)	
Residual CF_4	331,716-580,503 $kg \cdot a^{-1}$	$2.438 \cdot 10^9$-$4.266 \cdot 10^9$ $kg \cdot a^{-1}$	1382 $kg \cdot a^{-1}$	$10.157 \cdot 10^6$ $kg \cdot a^{-1}$
Secondary CO_2	55,280-179.660 $kg \cdot a^{-1}$	55,280-179,660 $kg \cdot a^{-1}$	344,807 $kg \cdot a^{-1}$	344,807 $kg \cdot a^{-1}$
N_2O formation	78.5 $kg \cdot a^{-1}$ (5 ppm ***)	24,330 $kg \cdot a^{-1}$	25.1 $kg \cdot a^{-1}$ (1.6 ppm ***)	7786 $kg \cdot a^{-1}$
Sum		**$2.438 \cdot 10^9$-$4.266 \cdot 10^9$ $kg \cdot a^{-1}$**		**$14.234 \cdot 10^6$ $kg \cdot a^{-1}$**
Reduction potential	**0 $kg \cdot a^{-1}$**		**$2.424 \cdot 10^9$-$4.252 \cdot 10^9$ $kg \cdot a^{-1}$ or 99.4–99.7%**	

7. Conclusions and Perspectives

The present results show that both non-thermal and thermal plasmas can be used in a wide range of applications in waste gas treatment. Nevertheless, their application is subject to a number of obstacles that need to be resolved first.

(1) Previous investigations were almost exclusively carried out at laboratory scale. Reliable scale-up factors for the transfer into industrial-scale systems are almost completely missing. The applied laboratory-scale leads to very high SIE values, so that an economic estimation is mostly not possible.
(2) Most studies deal with the treatment of individual components, but treatment of VOC mixtures is mainly not addressed. Removal efficiencies of single compounds are probably not transferable to situation in VOC mixtures, since VOC compounds compete for reactive plasma species, on the one hand, and, on the other hand, reactive interactions between different pollutants may occur.
(3) The effect of interfering compounds in real waste gases like water saturated or oversaturated conditions, aerosols, dust and salt particles have not been sufficiently investigated.
(4) Methods to reduce the energy demand of plasma systems like intermittent plasmas, heat recovery (only thermal plasma) or process combinations with low-energy process like biological approaches have hardly been investigated so far.
(5) There is a clear lack of experiences about thermal (only thermal plasma) and chemical long-term stability of the materials used. Accordingly, the maintenance intervals are currently quite short.
(6) Recently developed catalysts are mostly nanoparticles not suitable for waste gas applications. Furthermore, their production process is complex, and therefore, production and application are not possible under economic aspects.

According to these restrictions, plasma processes are currently only used frequently in niches, such as treatment of CFCs or clean room air treatment. However, the research results presented here impressively underline the possibility of the large-scale application of these processes. Thus, there is a need to catch up on these six aspects before the objective of industrial-scale application is achieved, especially since these processes appear to be very interesting compared to conventional waste air treatment processes under economic and ecological aspects.

Author Contributions: Conceptualization and methodology, C.D. and B.G.; calculations, C.D.; investigation, C.D. and B.G.; writing—original draft preparation, review and editing, C.D.; visualization, C.D.; project administration, C.D. All authors have read and agreed to the published version of the manuscript.

Funding: This research was funded by the German Federal Ministry of Education and Research and the Project Management Agency in the DLR (grant numbers 01LY1203/01LY1604) and the German Federal Ministry for Economic Affairs and Energy and the Project Management Agency AIF (grant numbers KF2533402RH3, ZF4073805CM7 and ZF4073806DF9).

Acknowledgments: We would like to thank Andreas Schulz for spectroscopic analysis and Daniel Dobslaw for gas analysis (both University of Stuttgart).

Conflicts of Interest: The authors declare no conflict of interest.

References

1. Moreno Cárdenas, F.; Cristancho Sánchez, S.; Vargas Domínguez, S. The grand aurorae borealis seen in Colombia in 1859. *Adv. Space Res.* **2016**, *57*, 257–267. [CrossRef]
2. Corson, D.W. Pierre Poliniere, Francis Hauksbee, and Electroluminescence: A Case of Simultaneous Discovery. *ISIS* **1968**, *59*, 402–413.
3. Pekárek, S. DC corona ozone generation enhanced by TiO_2 photocatalyst. *Eur. Phys. J. D* **2008**, *50*, 171–175. [CrossRef]
4. Mott-Smith, H.M. History of "plasmas". *Nature* **1971**, *233*, 219. [CrossRef]
5. Chen, F.F. Plasma Applications. In *Introduction to Plasma Physics and Controlled Fusion*; Chen, F.F., Ed.; Springer International Publishing: Cham, Switzerland, 2016; pp. 355–411, ISBN 978-3-319-22308-7.

6. Stryczewska, H.D. Supply Systems of Non-Thermal Plasma Reactors. Construction Review with Examples of Applications. *Appl. Sci.* **2020**, *10*, 3242. [CrossRef]
7. López, M.; Calvo, T.; Prieto, M.; Múgica-Vidal, R.; Muro-Fraguas, I.; Alba-Elías, F.; Alvarez-Ordóñez, A. A Review on Non-thermal Atmospheric Plasma for Food Preservation: Mode of Action, Determinants of Effectiveness, and Applications. *Front. Microbiol.* **2019**, *10*, 622. [CrossRef]
8. Clothiaux, E.J.; Koropchak, J.A.; Moore, R.R. Decomposition of an organophosphorus material in a silent electrical discharge. *Plasma Chem. Plasma Process.* **1984**, *4*, 15–20. [CrossRef]
9. Fraser, M.E.; Sheinson, R.S. Electric discharge-induced oxidation of hydrogen cyanide. *Plasma Chem. Plasma Process.* **1986**, *6*, 27–38. [CrossRef]
10. Cal, M.P.; Schluep, M. Destruction of benzene with non-thermal plasma in dielectric barrier discharge reactors. *Environ. Prog.* **2001**, *20*, 151–156. [CrossRef]
11. Fang, H.J.; Hou, H.Q.; Xia, L.Y.; Shu, X.H.; Zhang, R.X. A combined plasma photolysis (CPP) method for removal of CS2 from gas streams at atmospheric pressure. *Chemosphere* **2007**, *69*, 1734–1739. [CrossRef]
12. Li, S.; Dang, X.; Yu, X.; Abbas, G.; Zhang, Q.; Cao, L. The application of dielectric barrier discharge non-thermal plasma in VOCs abatement: A review. *Chem. Eng. J.* **2020**, *388*, 124275. [CrossRef]
13. Schiavon, M.; Torretta, V.; Casazza, A.; Ragazzi, M. Non-thermal Plasma as an Innovative Option for the Abatement of Volatile Organic Compounds: A Review. *Water Air Soil Pollut.* **2017**, 228. [CrossRef]
14. Dobslaw, D.; Ortlinghaus, O.; Dobslaw, C. A combined process of non-thermal plasma and a low-cost mineral adsorber for VOC removal and odor abatement in emissions of organic waste treatment plants. *J. Environ. Chem. Eng.* **2018**, *6*, 2281–2289. [CrossRef]
15. George, A.; Shen, B.; Craven, M.; Wang, Y.; Kang, D.; Wu, C.; Tu, X. A Review of Non-Thermal Plasma Technology: A novel solution for CO_2 conversion and utilization. *Renew. Sustain. Energy Rev.* **2021**, *135*, 109702. [CrossRef]
16. Dobslaw, D. *Herausforderungen in der Biologischen und Nicht-Biologischen Abluftreinigung*; University of Stuttgart: Stuttgart, Germany, 2020. [CrossRef]
17. Marotta, E.; Schiorlin, M.; Rea, M.; Paradisi, C. Products and mechanisms of the oxidation of organic compounds in atmospheric air plasmas. *J. Phys. D Appl. Phys.* **2010**, *43*, 124011. [CrossRef]
18. Marotta, E.; Scorrano, G.; Paradisi, C. Ionic Reactions of Chlorinated Volatile Organic Compounds in Air Plasma at Atmospheric Pressure. *Plasma Process. Polym.* **2005**, *2*, 209–217. [CrossRef]
19. Cheng, Z.-W.; Zhang, L.-L.; Chen, J.-M.; Yu, J.-M.; Gao, Z.-L.; Jiang, Y.-F. Treatment of gaseous alpha-pinene by a combined system containing photo oxidation and aerobic biotrickling filtration. *J. Hazard. Mater.* **2011**, *192*, 1650–1658. [CrossRef]
20. Istadi, I.; Saidina Amin, N.A. Catalytic-Dielectric Barrier Discharge Plasma Reactor for Methane and Carbon Dioxide Conversion. *Bull. Chem. React. Eng. Catal.* **2007**, *2*, 37–44. [CrossRef]
21. Kasinathan, P.; Park, S.; Choi, W.C.; Hwang, Y.K.; Chang, J.-S.; Park, Y.-K. Plasma-Enhanced Methane Direct Conversion over Particle-Size Adjusted MOx/Al2O3 (M = Ti and Mg) Catalysts. *Plasma Chem. Plasma Process.* **2014**, *34*, 1317–1330. [CrossRef]
22. Kogelschatz, U.; Eliasson, B.; Egli, W. Dielectric-Barrier Discharges. Principle and Applications. *J. Phys. IV* **1997**, *7*, C4–C47. [CrossRef]
23. Liu, C.; Cui, N.; Brown, N.M.D.; Meenan, B.J. Effects of DBD plasma operating parameters on the polymer surface modification. *Surf. Coat. Technol.* **2004**, *185*, 311–320. [CrossRef]
24. Liu, J.; Zhu, X.; Li, X.; Li, K.; Shi, C.; Zhu, A. Effect of O2/CH4 ratio on the optimal specific-energy-input (SEI) for oxidative reforming of biogas in a plasma-shade reactor. *J. Energy Chem.* **2013**, *22*, 681–684. [CrossRef]
25. Mfopara, A.; Kirkpatrick, M.J.; Odic, E. Dilute Methane Treatment by Atmospheric Pressure Dielectric Barrier Discharge: Effects of Water Vapor. *Plasma Chem. Plasma Process.* **2009**, *29*, 91–102. [CrossRef]
26. Nozaki, T.; Okazaki, K. Innovative Methane Conversion Technology Using Atmospheric Pressure Non-thermal Plasma. *J. Jpn. Pet. Inst.* **2011**, *54*, 146–158. [CrossRef]
27. Sultana, S.; Vandenbroucke, A.; Leys, C.; de Geyter, N.; Morent, R. Abatement of VOCs with Alternate Adsorption and Plasma-Assisted Regeneration: A Review. *Catalysts* **2015**, *5*, 718–746. [CrossRef]
28. Wu, J.; Xia, Q.; Wang, H.; Li, Z. Catalytic performance of plasma catalysis system with nickel oxide catalysts on different supports for toluene removal: Effect of water vapor. *Appl. Catal. B Environ.* **2014**, *156–157*, 265–272. [CrossRef]

29. Zheng, X.; Tan, S.; Dong, L.; Li, S.; Chen, H. Plasma-assisted catalytic dry reforming of methane: Highly catalytic performance of nickel ferrite nanoparticles embedded in silica. *J. Power Sources* **2015**, *274*, 286–294. [CrossRef]
30. Sivachandiran, L.; Thevenet, F.; Rousseau, A. Isopropanol removal using MnXOY packed bed non-thermal plasma reactor: Comparison between continuous treatment and sequential sorption/regeneration. *Chem. Eng. J.* **2015**, *270*, 327–335. [CrossRef]
31. Dobslaw, D.; Schulz, A.; Helbich, S.; Dobslaw, C.; Engesser, K.-H. VOC removal and odor abatement by a low-cost plasma enhanced biotrickling filter process. *J. Environ. Chem. Eng.* **2017**, *5*, 5501–5511. [CrossRef]
32. Dobslaw, D.; Ortlinghaus, O. Biological Waste Air and Waste Gas Treatment: Overview, Challenges, Operational Efficiency, and Current Trends. *Sustainability* **2020**, *12*, 8577. [CrossRef]
33. Hoeben, W.F.L.M.; Beckers, F.J.C.M.; Pemen, A.J.M.; van Heesch, E.J.M.; Kling, W.L. Oxidative degradation of toluene and limonene in air by pulsed corona technology. *J. Phys. D Appl. Phys.* **2012**, *45*, 55202. [CrossRef]
34. Lee, H.; Lee, D.-H.; Song, Y.-H.; Choi, W.C.; Park, Y.-K.; Kim, D.H. Synergistic effect of non-thermal plasma–catalysis hybrid system on methane complete oxidation over Pd-based catalysts. *Chem. Eng. J.* **2015**, *259*, 761–770. [CrossRef]
35. Jarrige, J.; Vervisch, P. Decomposition of three volatile organic compounds by nanosecond pulsed corona discharge: Study of by-product formation and influence of high voltage pulse parameters. *J. Appl. Phys.* **2006**, *99*, 113303. [CrossRef]
36. Gandhi, M.S.; Mok, Y.S.; Lee, S.B.; Park, H. Effect of various parameters for butane decomposition under ambient temperature in a dielectric barrier discharge non-thermal plasma reactor. *J. Taiwan Inst. Chem. Eng.* **2013**, *44*, 786–794. [CrossRef]
37. Wandell, R.J.; Bresch, S.; Hsieh, K.; Alabugin, I.V.; Locke, B.R. Formation of Alcohols and Carbonyl Compounds From Hexane and Cyclohexane With Water in a Liquid Film Plasma Reactor. *IEEE Trans. Plasma Sci.* **2014**, *42*, 1195–1205. [CrossRef]
38. Prantsidou, M.; Whitehead, J.C. The Chemistry of Gaseous Dodecane Degradation in a BaTiO3 Packed-Bed Plasma Reactor. *Plasma Chem. Plasma Process.* **2015**, *35*, 159–172. [CrossRef]
39. Iijima, S.; Nakamura, M.; Yokoi, A.; Kubota, M.; Huang, L.; Matsuda, H. Decomposition of dichloromethane and in situ alkali absorption of resulting halogenated products by a packed-bed non-thermal plasma reactor. *J. Mater. Cycles Waste Manag.* **2011**, *13*, 206–212. [CrossRef]
40. Aerts, R.; Tu, X.; de Bie, C.; Whitehead, J.C.; Bogaerts, A. An Investigation into the Dominant Reactions for Ethylene Destruction in Non-Thermal Atmospheric Plasmas. *Plasma Process. Polym.* **2012**, *9*, 994–1000. [CrossRef]
41. Abedi, K.; Ghorbani-Shahna, F.; Jaleh, B.; Bahrami, A.; Yarahmadi, R. Enhanced performance of non-thermal plasma coupled with TiO2/GAC for decomposition of chlorinated organic compounds: Influence of a hydrogen-rich substance. *J. Environ. Health Sci. Eng.* **2014**, *12*, 119. [CrossRef]
42. Vandenbroucke, A.M.; Mora, M.; Jiménez-Sanchidrián, C.; Romero-Salguero, F.J.; de Geyter, N.; Leys, C.; Morent, R. TCE abatement with a plasma-catalytic combined system using MnO2 as catalyst. *Appl. Catal. B Environ.* **2014**, *156–157*, 94–100. [CrossRef]
43. Vandenbroucke, A.M.; Aerts, R.; van Gaens, W.; de Geyter, N.; Leys, C.; Morent, R.; Bogaerts, A. Modeling and Experimental Study of Trichloroethylene Abatement with a Negative Direct Current Corona Discharge. *Plasma Chem. Plasma Process.* **2015**, *35*, 217–230. [CrossRef]
44. Vandenbroucke, A.M.; Morent, R.; de Geyter, N.; Leys, C. Non-thermal plasmas for non-catalytic and catalytic VOC abatement. *J. Hazard. Mater.* **2011**, *195*, 30–54. [CrossRef] [PubMed]
45. Vandenbroucke, A.M.; Nguyen Dinh, M.T.; Nuns, N.; Giraudon, J.-M.; de Geyter, N.; Leys, C.; Lamonier, J.-F.; Morent, R. Combination of non-thermal plasma and Pd/LaMnO3 for dilute trichloroethylene abatement. *Chem. Eng. J.* **2016**, *283*, 668–675. [CrossRef]
46. Magureanu, M.; Mandache, N.B.; Parvulescu, V.I.; Subrahmanyam, C.; Renken, A.; Kiwi-Minsker, L. Improved performance of non-thermal plasma reactor during decomposition of trichloroethylene: Optimization of the reactor geometry and introduction of catalytic electrode. *Appl. Catal. B Environ.* **2007**, *74*, 270–277. [CrossRef]
47. Oda, T.; Yamaji, K.; Takahashi, T. Decomposition of Dilute Trichloroethylene by Nonthermal Plasma Processing—Gas Flow Rate, Catalyst, and Ozone Effect. *IEEE Trans. Ind. Appl.* **2004**, *40*, 430–436. [CrossRef]

48. Zhu, X.; Liu, S.; Cai, Y.; Gao, X.; Zhou, J.; Zheng, C.; Tu, X. Post-plasma catalytic removal of methanol over Mn–Ce catalysts in an atmospheric dielectric barrier discharge. *Appl. Catal. B Environ.* **2016**, *183*, 124–132. [CrossRef]
49. Sivachandiran, L.; Thevenet, F.; Gravejat, P.; Rousseau, A. Isopropanol saturated TiO2 surface regeneration by non-thermal plasma: Influence of air relative humidity. *Chem. Eng. J.* **2013**, *214*, 17–26. [CrossRef]
50. Zhu, X.; Gao, X.; Qin, R.; Zeng, Y.; Qu, R.; Zheng, C.; Tu, X. Plasma-catalytic removal of formaldehyde over Cu–Ce catalysts in a dielectric barrier discharge reactor. *Appl. Catal. B Environ.* **2015**, *170–171*, 293–300. [CrossRef]
51. Maciuca, A.; Batiot-Dupeyrat, C.; Tatibouët, J.-M. Synergetic effect by coupling photocatalysis with plasma for low VOCs concentration removal from air. *Appl. Catal. B Environ.* **2012**, *125*, 432–438. [CrossRef]
52. Ragazzi, M.; Tosi, P.; Rada, E.C.; Torretta, V.; Schiavon, M. Effluents from MBT plants: Plasma techniques for the treatment of VOCs. *Waste Manag.* **2014**, *34*, 2400–2406. [CrossRef]
53. Zhu, X.; Zhang, S.; Yang, Y.; Zheng, C.; Zhou, J.; Gao, X.; Tu, X. Enhanced performance for plasma-catalytic oxidation of ethyl acetate over La1-xCexCoO3+δ catalysts. *Appl. Catal. B Environ.* **2017**, *213*, 97–105. [CrossRef]
54. Ye, Z.; Gu, A.; Zhang, R.; Hou, H. Removal of Isobutyl Acetate in Flowed Air Stream with DBD Plasmas. Removal of Isobutyl Acetate in Flowed Air Stream with DBD Plasmas. In Proceedings of the 2010 4th International Conference on Bioinformatics and Biomedical Engineering (iCBBE), Chengdu, China, 18–20 June 2010; Ye, Z., Gu, A., Zhang, R., Hou, H., Eds.; IEEE: Piscataway, NJ, USA, 2010; pp. 1–5, ISBN 978-1-4244-4712-1.
55. Lu, B.; Zhang, X.; Yu, X.; Feng, T.; Yao, S. Catalytic oxidation of benzene using DBD corona discharges. *J. Hazard. Mater.* **2006**, *137*, 633–637. [CrossRef] [PubMed]
56. Schmid, S.; Jecklin, M.C.; Zenobi, R. Degradation of volatile organic compounds in a non-thermal plasma air purifier. *Chemosphere* **2010**, *79*, 124–130. [CrossRef]
57. Hoeben, W.F.L.M.; Boekhoven, W.; Beckers, F.J.C.M.; van Heesch, E.J.M.; Pemen, A.J.M. Partial oxidation of methane by pulsed corona discharges. *J. Phys. D Appl. Phys.* **2014**, *47*, 355202. [CrossRef]
58. Ognier, S.; Youssef, J.; Cavadias, S.; Amouroux, J. SFGP 2007—A New Concept for the Abatement of Volatile Organic Compounds by a Two-Stage Process Combining Non-Thermal Plasma Treatment and Filtration. *Int. J. Chem. React. Eng.* **2008**, 6. [CrossRef]
59. van Durme, J.; Dewulf, J.; Sysmans, W.; Leys, C.; van Langenhove, H. Abatement and degradation pathways of toluene in indoor air by positive corona discharge. *Chemosphere* **2007**, *68*, 1821–1829. [CrossRef] [PubMed]
60. Lu, M.; Huang, R.; Wu, J.; Fu, M.; Chen, L.; Ye, D. On the performance and mechanisms of toluene removal by FeOx/SBA-15-assisted non-thermal plasma at atmospheric pressure and room temperature. *Catal. Today* **2015**, *242*, 274–286. [CrossRef]
61. Anderson, G.K.; Snyder, H.; Coogan, J. Oxidation of styrene in a silent discharge plasma. *Plasma Chem. Plasma Process.* **1999**, *19*, 131–151. [CrossRef]
62. Chang, C.-L.; Bai, H.; Lu, S.-J. Destruction of Styrene in an Air Stream by Packed Dielectric Barrier Discharge Reactors. *Plasma Chem. Plasma Process.* **2005**, *25*, 641–657. [CrossRef]
63. Wei, Z.S.; Li, H.Q.; He, J.C.; Ye, Q.H.; Huang, Q.R.; Luo, Y.W. Removal of dimethyl sulfide by the combination of non-thermal plasma and biological process. *Bioresour. Technol.* **2013**, *146*, 451–456. [CrossRef]
64. Mitrović, T.; Lazović, S.; Nastasijević, B.; Pašti, I.A.; Vasić, V.; Lazarević-Pašti, T. Non-thermal plasma needle as an effective tool in dimethoate removal from water. *J. Environ. Manag.* **2019**, *246*, 63–70. [CrossRef] [PubMed]
65. Iervolino, G.; Vaiano, V.; Palma, V. Enhanced removal of water pollutants by dielectric barrier discharge non-thermal plasma reactor. *Sep. Purif. Technol.* **2019**, *215*, 155–162. [CrossRef]
66. Murugesan, P.; Moses, J.A.; Anandharamakrishnan, C. Water decontamination using non-thermal plasma: Concepts, applications, and prospects. *J. Environ. Chem. Eng.* **2020**, *8*, 104377. [CrossRef]
67. Chen, H.; Mu, Y.; Xu, S.; Xu, S.; Hardacre, C.; Fan, X. Recent advances in non-thermal plasma (NTP) catalysis towards C1 chemistry. *Chin. J. Chem. Eng.* **2020**, *28*, 2010–2021. [CrossRef]
68. Brisset, J.-L.; Pawlat, J. Chemical Effects of Air Plasma Species on Aqueous Solutes in Direct and Delayed Exposure Modes: Discharge, Post-discharge and Plasma Activated Water. *Plasma Chem. Plasma Process.* **2016**, *36*, 355–381. [CrossRef]

69. Lee, D.H.; Song, Y.-H.; Kim, K.-T.; Lee, J.-O. Comparative Study of Methane Activation Process by Different Plasma Sources. *Plasma Chem. Plasma Process.* **2013**, *33*, 647–661. [CrossRef]
70. Nozaki, T.; Okazaki, K. Non-thermal plasma catalysis of methane: Principles, energy efficiency, and applications. *Catal. Today* **2013**, *211*, 29–38. [CrossRef]
71. Zhang, K.; Harvey, A.P. CO_2 decomposition to CO in the presence of up to 50% O_2 using a non-thermal plasma at atmospheric temperature and pressure. *Chem. Eng. J.* **2021**, *405*, 126625. [CrossRef]
72. Bogaerts, A.; Tu, X.; Whitehead, J.C.; Centi, G.; Lefferts, L.; Guaitella, O.; Azzolina-Jury, F.; Kim, H.-H.; Murphy, A.B.; Schneider, W.F.; et al. The 2020 plasma catalysis roadmap. *J. Phys. D Appl. Phys.* **2020**, *53*, 443001. [CrossRef]
73. Amouroux, J.; Talbot, J. Etude des conditions de pyrolyse du méthane dans un plasma inductif d'argon: Conditions for methane pyrolysis in an inductive plasma of argon. *Ann. Chim.* **1968**, *3*, 219–233.
74. Gautier, M.; Rohani, V.; Fulcheri, L. Direct decarbonization of methane by thermal plasma for the production of hydrogen and high value-added carbon black. *Int. J. Hydrogen Energy* **2017**, *42*, 28140–28156. [CrossRef]
75. Abbas, H.F.; Wan Daud, W.M.A. Hydrogen production by methane decomposition: A review. *Int. J. Hydrogen Energy* **2010**, *35*, 1160–1190. [CrossRef]
76. Sikarwar, V.S.; Hrabovský, M.; van Oost, G.; Pohořelý, M.; Jeremiáš, M. Progress in waste utilization via thermal plasma. *Prog. Energy Combust. Sci.* **2020**, *81*, 100873. [CrossRef]
77. Montoro-Damas, A.M.; Brey, J.J.; Rodríguez, M.A.; González-Elipe, A.R.; Cotrino, J. Plasma reforming of methane in a tunable ferroelectric packed-bed dielectric barrier discharge reactor. *J. Power Sources* **2015**, *296*, 268–275. [CrossRef]
78. Saleem, F.; Harris, J.; Zhang, K.; Harvey, A. Non-thermal plasma as a promising route for the removal of tar from the product gas of biomass gasification—A critical review. *Chem. Eng. J.* **2020**, *382*, 122761. [CrossRef]
79. Mizuno, A. Industrial applications of atmospheric non-thermal plasma in environmental remediation. *Plasma Phys. Control. Fusion* **2007**, *49*, A1–A15. [CrossRef]
80. Müller, S.; Zahn, R.-J. Air Pollution Control by Non-Thermal Plasma. *Contrib. Plasma Phys.* **2007**, *47*, 520–529. [CrossRef]
81. Chang, J.-S.; Looy, P.C.; Nagai, K.; Yoshioka, T.; Aoki, S.; Maezawa, A. Preliminary pilot plant tests of a corona discharge-electron beam hybrid combustion flue gas cleaning system. *IEEE Trans. Ind. Appl.* **1996**, *32*, 131–137. [CrossRef]
82. Chen, J.; Yang, J.; Pan, H.; Su, Q.; Liu, Y.; Shi, Y. Abatement of malodorants from pesticide factory in dielectric barrier discharges. *J. Hazard. Mater.* **2010**, *177*, 908–913. [CrossRef]
83. Kuwahara, T.; Okubo, M.; Kuroki, T.; Kametaka, H.; Yamamoto, T. Odor removal characteristics of a laminated film-electrode packed-bed nonthermal plasma reactor. *Sensors* **2011**, *11*, 5529–5542. [CrossRef]
84. Liang, W.-J.; Ma, L.; Li, J.; Li, J.-X.; Zheng, F. Control of Hydrogen Sulfide by a Wire-Tube Dielectric Barrier Discharge AC Plasma Reactor. *Clean Soil Air Water* **2012**, *40*, 586–591. [CrossRef]
85. Park, C.W.; Byeon, J.H.; Yoon, K.Y.; Park, J.H.; Hwang, J. Simultaneous removal of odors, airborne particles, and bioaerosols in a municipal composting facility by dielectric barrier discharge. *Sep. Purif. Technol.* **2011**, *77*, 87–93. [CrossRef]
86. Xia, L.; Huang, L.; Shu, X.; Zhang, R.; Dong, W.; Hou, H. Removal of ammonia from gas streams with dielectric barrier discharge plasmas. *J. Hazard. Mater.* **2008**, *152*, 113–119. [CrossRef] [PubMed]
87. Yang, J.-t.; Shi, Y.; Chen, J.; Su, Q.-f.; Wang, D.-h.; Cao, J. Decomposition of dimethyl sulfide in a wire-cylinder pulse corona reactor. *J. Zhejiang Univ. Sci. A* **2009**, *10*, 127–132. [CrossRef]
88. Zhu, C.; Wang, X.; Huang, Q.; Huang, L.; Xie, J.; Qing, C.; Chen, T. Removal of gaseous carbon bisulfide using dielectric barrier discharge plasmas combined with TiO2 coated attapulgite catalyst. *Chem. Eng. J.* **2013**, *225*, 567–573. [CrossRef]
89. Preis, S.; Klauson, D.; Gregor, A. Potential of electric discharge plasma methods in abatement of volatile organic compounds originating from the food industry. *J. Environ. Manag.* **2013**, *114*, 125–138. [CrossRef]
90. Benstaali, B.; Moussa, D.; Addou, A.; Brisset, J.-L. Plasma treatment of aqueous solutes: Some chemical properties of a gliding arc in humid air. *Eur. Phys. J. Appl. Phys.* **1998**, *4*, 171–179. [CrossRef]
91. Jayasena, D.D.; Kim, H.J.; Yong, H.I.; Park, S.; Kim, K.; Choe, W.; Jo, C. Flexible thin-layer dielectric barrier discharge plasma treatment of pork butt and beef loin: Effects on pathogen inactivation and meat-quality attributes. *Food Microbiol.* **2015**, *46*, 51–57. [CrossRef] [PubMed]

92. Kim, H.-J.; Yong, H.I.; Park, S.; Choe, W.; Jo, C. Effects of dielectric barrier discharge plasma on pathogen inactivation and the physicochemical and sensory characteristics of pork loin. *Curr. Appl. Phys.* **2013**, *13*, 1420–1425. [CrossRef]
93. Kim, H.-J.; Yong, H.I.; Park, S.; Kim, K.; Choe, W.; Jo, C. Microbial safety and quality attributes of milk following treatment with atmospheric pressure encapsulated dielectric barrier discharge plasma. *Food Control* **2015**, *47*, 451–456. [CrossRef]
94. Laroussi, M.; Mendis, D.A.; Rosenberg, M. Plasma interaction with microbes. *New J. Phys.* **2003**, *5*, 41. [CrossRef]
95. Pelletier, J. La stérilisation par le procédé plasma. *Agressologie* **1992**, *33*, 105–110. [PubMed]
96. Ohshima, T.; Sato, M.; Saito, M. Selective release of intracellular protein using pulsed electric field. *J. Electrost.* **1995**, *35*, 103–112. [CrossRef]
97. Shintani, H. Inactivation of Bacterial Spore, Endotoxin, Lipid A, Normal Prion and Abnormal Prion by Exposures to Several Sorts of Gases Plasma. *Biocontrol. Sci.* **2016**, *21*, 1–12. [CrossRef] [PubMed]
98. Yu, H.; Xiu, Z.L.; Ren, C.S.; Zhang, J.L.; de Wang, Z.; Wang, Y.N.; Ma, T.C. Inactivation of yeast by dielectric barrier discharge (DBD) plasma in helium at atmospheric pressure. *IEEE Trans. Plasma Sci.* **2005**, *33*, 1405–1409. [CrossRef]
99. Moreau, M.; Feuilloley, M.G.J.; Veron, W.; Meylheuc, T.; Chevalier, S.; Brisset, J.-L.; Orange, N. Gliding arc discharge in the potato pathogen Erwinia carotovora subsp. atroseptica: Mechanism of lethal action and effect on membrane-associated molecules. *Appl. Environ. Microbiol.* **2007**, *73*, 5904–5910. [CrossRef]
100. Shen, J.; Tian, Y.; Li, Y.; Ma, R.; Zhang, Q.; Zhang, J.; Fang, J. Bactericidal Effects against *S. aureus* and Physicochemical Properties of Plasma Activated Water stored at different temperatures. *Sci. Rep.* **2016**, *6*, 28505. [CrossRef]
101. Lee, J.; Bong, C.; Bae, P.K.; Abafog, A.T.; Baek, S.H.; Shin, Y.-B.; Park, M.S.; Park, S. Fast and easy disinfection of coronavirus-contaminated face masks using ozone gas produced by a dielectric barrier discharge plasma generator. *medRxiv* **2020**. [CrossRef]
102. Bekeschus, S.; Kramer, A.; Suffredini, E.; von Woedtke, T.; Colombo, V. Gas Plasma Technology—An Asset to Healthcare During Viral Pandemics Such as the COVID-19 Crisis? *IEEE Trans. Radiat. Plasma Med. Sci.* **2020**, *4*, 391–399. [CrossRef]
103. Chung, W.-C.; Mei, D.-H.; Tu, X.; Chang, M.-B. Removal of VOCs from gas streams via plasma and catalysis. *Catal. Rev.* **2019**, *61*, 270–331. [CrossRef]
104. Adelodun, A.A. Influence of Operation Conditions on the Performance of Non-thermal Plasma Technology for VOC Pollution Control. *J. Ind. Eng. Chem.* **2020**, *92*, 41–55. [CrossRef]
105. Guo, T.; Cheng, G.; Tan, G.; Xu, L.; Huang, Z.; Cheng, P.; Zhou, Z. Real-time analysis of intermediate products from non-thermal plasma degradation of ethyl acetate in air using PTR-MS: Performance evaluation and mechanism study. *Chemosphere* **2020**, *264*, 128430. [CrossRef] [PubMed]
106. Verein Deutscher Ingenieure VDI. *Process Gas and Waste Gas Cleaning by Cold Plasma—Barrier discharge, Corona discharge, UV radiation; VDI guideline no. 2441*; Beuth Verlag GmbH: Berlin, Germany, 2016.
107. Choi, S.; Lee, H.S.; Kim, S.W.; Park, D.-W.; Hong, S.H. Thermal Plasma Analysis for PFCs Pyrolysis Process on a Large Scale. *J. Korean Phys. Soc.* **2009**, *55*, 1819–1824. [CrossRef]
108. Choi, S.; Hong, S.H.; Lee, H.S.; Watanabe, T. A comparative study of air and nitrogen thermal plasmas for PFCs decomposition. *Chem. Eng. J.* **2012**, *185–186*, 193–200. [CrossRef]
109. Jeništa, J.; Takana, H.; Uehara, S.; Nishiyama, H.; Bartlová, M.; Aubrecht, V.; Murphy, A.B. Modeling of inhomogeneous mixing of plasma species in argon–steam arc discharge. *J. Phys. D Appl. Phys.* **2018**, *51*, 45202. [CrossRef]
110. Dobslaw, D.; Dobslaw, C. *Strahlungsgekühlte, Thermische Wasserdampfplasmaanlage zur Behandlung Perfluorierter Abluftströme—"StrahlWaBe": Schlussbericht zu Nr. 8.2 des Forschungsvorhabens*; German National Library of Science and Technology: Hannover, Germany, 2019. [CrossRef]
111. Kim, D.-y.; Park, D.W. Decomposition of PFCs by steam plasma at atmospheric pressure. *Surf. Coat. Technol.* **2008**, *202*, 5280–5283. [CrossRef]
112. Suris, A.L. Investigation of high-temperature steam–air reagents for plasma waste treatment processes. *Found. Chem. Eng.* **2017**, *51*, 348–351. [CrossRef]
113. Sharma, R.; Singh, G.; Singh, K. Modelling of the Thermophysical Properties in Ar-He-H2 Thermal Plasmas with Electronic Excitation. *J. Korean Phys. Soc.* **2011**, *58*, 1703–1707. [CrossRef]

114. Tao, X.; Bai, M.; Wu, Q.; Huang, Z.; Yin, Y.; Dai, X. CO_2 reforming of CH4 by binode thermal plasma. *Int. J. Hydrogen Energy* **2009**, *34*, 9373–9378. [CrossRef]
115. Tao, X.; Qi, F.; Yin, Y.; Dai, X. CO_2 reforming of CH4 by combination of thermal plasma and catalyst. *Int. J. Hydrogen Energy* **2008**, *33*, 1262–1265. [CrossRef]
116. Han, S.-H.; Park, H.-W.; Kim, T.-H.; Park, D.-W. Large scale treatment of perfluorocompounds using a thermal plasma scrubber. *Clean Technol.* **2011**, *17*, 250–258. [CrossRef]
117. Lee, C.H.; Chun, Y.N. Reduction of Tetrafluoromethane using a Waterjet Gliding Arc Plasma. *Korean Chem. Eng. Res.* **2011**, *49*, 485–490. [CrossRef]
118. Dobslaw, D.; Helbich, S.; Dobslaw, C.; Glocker, B. *Einsatz Eines Strahlungsgekühlten, Thermischen Wasserdampfplasmas zur Behandlung von Treibhausrelevanten, Perfluorierten Abluftströmen. 5. VDI-Fachtagung Emissionsminderung 2018 Stand—Konzepte—Fortschritte, Nürnberg, 12./13.6.2018*; VDI Verlag GmbH: Düsseldorf, Germany, 2018; ISBN 978-3-18-092327-7.
119. Niemira, B.A. Cold plasma decontamination of foods. *Annu. Rev. Food Sci. Technol.* **2012**, *3*, 125–142. [CrossRef] [PubMed]
120. Hrabovsky, M. Thermal Plasma Gasification of Biomass. In *Progress in Biomass and Bioenergy Production*; Shaukat, S., Ed.; InTech: London, UK, 2011; ISBN 978-953-307-491-7.
121. Nishikawa, H.; Ibe, M.; Tanaka, M.; Ushio, M.; Takemoto, T.; Tanaka, K.; Tanahashi, N.; Ito, T. A treatment of carbonaceous wastes using thermal plasma with steam. *Vacuum* **2004**, *73*, 589–593. [CrossRef]
122. Kim, T.-H.; Choi, S.; Park, D.-W. Numerical simulation on the influence of water spray in thermal plasma treatment of CF4 gas. *Curr. Appl. Phys.* **2012**, *12*, 509–514. [CrossRef]
123. Saito, H.; Watanabe, T. Decomposition Mechanism of Fluorinated Compounds in Water Plasmas Generated Under Atmospheric Pressure. *Plasma Chem. Plasma Process.* **2010**, *30*, 813–829. [CrossRef]
124. Tianming, L.; Choi, S.; Watanabe, T. Discharge Characteristics of DC Arc Water Plasma for Environmental Applications. *Plasma Sci. Technol.* **2012**, *14*, 1097–1101. [CrossRef]
125. Watanabe, T.; Tsuru, T. Water plasma generation under atmospheric pressure for HFC destruction. *Thin Solid Film.* **2008**, *516*, 4391–4396. [CrossRef]
126. Watanabe, T. Water Plasmas for Environmental Application. In *Industrial Plasma Technology*; Kawai, Y., Ikegami, H., Sato, N., Matsuda, A., Uchino, K., Kuzuya, M., Mizuno, A., Eds.; Wiley-VCH Verlag GmbH & Co. KGaA: Weinheim, Germany, 2010; pp. 65–77, ISBN 9783527629749.
127. Glocker, B.; Nentwig, G.; Messerschmid, E. 1-40kW steam respectively multi gas thermal plasma torch system. *Vacuum* **2000**, *59*, 35–46. [CrossRef]
128. Watanabe, T. Acetone decomposition by water plasmas at atmospheric pressure. *Chem. Eng. Sci.* **2012**, *69*, 296–303. [CrossRef]
129. Choi, S.; Watanabe, T. Decomposition of 1-Decanol Emulsion by Water Thermal Plasma Jet. *IEEE Trans. Plasma Sci.* **2012**, *40*, 2831–2836. [CrossRef]
130. Chun, Y.N.; Lee, C.H. Development of a combined waterjet plasma scrubber for tetrafluoromethane and by-product removal. *Environ. Prog. Sustain. Energy* **2014**, *33*, 229–237. [CrossRef]
131. Ko, D.G.; Ko, S.J.; Choi, E.K.; Min, S.G.; Oh, S.H.; Jung, J.; Kim, B.M.; Im, I.-T. Perfluorocarbon Destruction and Removal Efficiency: Considering the Byproducts and Energy Consumption of an Abatement System for Microelectronics Manufacturing. *IEEE Trans. Semicond. Manufact.* **2014**, *27*, 456–461. [CrossRef]
132. Lim, M.S.; Kim, S.C.; Chun, Y.N. Decomposition of PFC gas using a water jet plasma. *J. Mech. Sci. Technol.* **2011**, *25*, 1845–1851. [CrossRef]
133. Sun, J.-W.; Park, D.-W. CF4 decomposition by thermal plasma processing. *Korean J. Chem. Eng.* **2003**, *20*, 476–481. [CrossRef]
134. Vartanian, V.; Goolsby, B.; Chatterjee, R.; Kachmarik, R.; Babbitt, D.; Reif, R.; Tonnis, E.J.; Graves, D. Reduction of Semiconductor Process Emissions by Reactive Gas Optimization. *IEEE Trans. Semicond. Manufact.* **2004**, *17*, 483–490. [CrossRef]
135. Yuan, M.-H.; Watanabe, T.; Chang, C.-Y. DC water plasma at atmospheric pressure for the treatment of aqueous phenol. *Environ. Sci. Technol.* **2010**, *44*, 4710–4715. [CrossRef]
136. Heberlein, J.; Murphy, A.B. Thermal plasma waste treatment. *J. Phys. D Appl. Phys.* **2008**, *41*, 53001. [CrossRef]
137. Zhang, L.; Wang, X.; Gong, B. Perfluorocarbon emissions from electrolytic reduction of rare earth metals in fluoride/oxide system. *Atmos. Pollut. Res.* **2018**, *9*, 61–65. [CrossRef]

138. Lee, S.-J.; Ryu, I.-S.; Jeon, S.-G.; Moon, S.-H. Emission sources and mitigation of fluorinated Non-CO_2 greenhouse gas in registered CDM projects. *Greenh. Gas Sci. Technol.* **2017**, *7*, 589–601. [CrossRef]
139. BMU. German Federal Ministry of Environment, Natur Conservation, Construction and Reactor Safety. In *Investitionen für ein Klimafreundliches Deutschland*; BMU: Bonn, Germany, 2008.
140. Dobslaw, D.; Schomburg, J.; Ortlinghaus, O.; Dobslaw, C.; Walker, M. *Abluftbehandlung durch eine Verfahrenskombination aus Nicht-Thermischen Plasma, Mineraladsorber und Wäscherstufe: Untersuchungen zur Machbarkeit und Effizienz einer Verfahrenskombination aus Nicht-Thermischen Plasma und Mineraladsorber zur Partiellen Oxidation von Abluftschadstoffen und einem Nachgeschalteten Biowäscher zur Eliminierung der Partiell Oxidierten Komponenten: "PIASTiC": Schlussbericht zu Nr. 8.2. des Forschungsvorhabens*; German National Library of Science and Technology: Hannover, Germany, 2015. [CrossRef]
141. Helbich, S.; Dobslaw, D.; Schulz, A.; Engesser, K.-H. Styrene and bioaerosol removal from waste air with combined biotrickling filter and DBD-plasma system. *Sustainability* **2020**, *12*. under review.
142. Martin, L.; Ognier, S.; Gasthauer, E.; Cavadias, S.; Dresvin, S.; Amouroux, J. Destruction of Highly Diluted Volatile Organic Components (VOCs) in Air by Dielectric Barrier Discharge and Mineral Bed Adsorption. *Energy Fuels* **2008**, *22*, 576–582. [CrossRef]
143. Jia, L.; Li, J. The experimental study on regenerative heat transfer in high temperature air combustion. *J. Therm. Sci.* **2004**, *13*, 366–370. [CrossRef]
144. Ou Yang, C.-F.; Kam, S.-H.; Liu, C.-H.; Tzou, J.; Wang, J.-L. Assessment of removal efficiency of perfluorocompounds (PFCs) in a semiconductor fabrication plant by gas chromatography. *Chemosphere* **2009**, *76*, 1273–1277. [CrossRef] [PubMed]
145. Kollbach, J.S.; Grömping, M. *Stickstoffrückbelastung. Stand der Technik 1996/97: Zukünftige Entwicklungen*; TK-Verlag: Neuruppin, Germany, 1996; ISBN 3-924511-85-3.

Publisher's Note: MDPI stays neutral with regard to jurisdictional claims in published maps and institutional affiliations.



© 2020 by the authors. Licensee MDPI, Basel, Switzerland. This article is an open access article distributed under the terms and conditions of the Creative Commons Attribution (CC BY) license (http://creativecommons.org/licenses/by/4.0/).